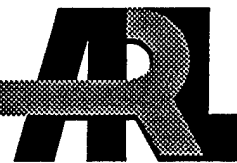


ARMY RESEARCH LABORATORY



Investigation of the CH₃CN-CO₂
Potential Energy Surface (PES)
Using Symmetry-Adapted
Perturbation Theory (SAPT)

by Hayes L. Williams, Betsy M. Rice, and Cary F. Chabalowski

ARL-TR-2301

September 2000

Approved for public release; distribution is unlimited.

DTIC QUALITY INDEXED 4

20001023 054

The findings in this report are not to be construed as an official Department of the Army position unless so designated by other authorized documents.

Citation of manufacturer's or trade names does not constitute an official endorsement or approval of the use thereof.

Destroy this report when it is no longer needed. Do not return it to the originator.

Army Research Laboratory

Aberdeen Proving Ground, MD 21005-5066

ARL-TR-2301

September 2000

Investigation of the CH₃CN-CO₂ Potential Energy Surface (PES) Using Symmetry-Adapted Perturbation Theory (SAPT)

Hayes L. Williams, Betsy M. Rice, and Cary F. Chabalowski
Weapons and Materials Research Directorate, ARL

Abstract

Symmetry-adapted perturbation theory (SAPT) has been used to investigate the intermolecular potential energy surface (PES) of CH₃CN-CO₂. A SAPT computation was performed for approximately 200 geometrical configurations using both a coarse grid in the five intermolecular coordinates as well as selected representative cuts. Four near-local minima are located on the PES. The deepest of these is -2.90 kcal/mol.

Acknowledgments

This work was partially supported by the Strategic Environmental Research and Development Program (SERDP), Project PP-695. The authors gratefully acknowledge the computer resources made available for this study on the Silicone Graphics Inc. (SGI) Power Challenge Array by the Department of Defense high-performance computing site at the U.S. Army Research Laboratory (ARL), Aberdeen Proving Ground, MD. This research was performed while Hayes Williams was a National Research Council postdoctoral associate at ARL, and he wishes to thank both organizations for their support. The authors would also like to thank Krzysztof Szalewicz and Bogumil Jeziorski for reading and commenting on the manuscript.

INTENTIONALLY LEFT BLANK.

Table of Contents

	<u>Page</u>
Acknowledgments	iii
List of Figures	vii
List of Tables	ix
1. Introduction	1
2. Method	2
3. Computational Details	6
4. Results and Discussion	14
5. Conclusions	38
6. References	41
Appendix: Supporting Information for Investigation of the CH₃CN-CO₂ Potential Energy Surface (PES) Using Symmetry-Adapted Perturbation Theory (SAPT)	45
Distribution List	77
Report Documentation Page	79

INTENTIONALLY LEFT BLANK.

List of Figures

<u>Figure</u>		<u>Page</u>
1. The Four Local Minimum Geometries Labeled as G1, G2, G3, and G4 in Table 2	7	
2. Graphical Representation of the Coordinate System Used to Specify the Dimer Configuration	10	
3. Cuts in R Through the PES for the Four Local Minimum Geometries Detailed in Table 2	19	
4a. SAPT Components Used in Equation (9) for a Range of R Values at and Around the Local Minimum Geometry G1	25	
4b. $E_{\text{int}}^{\text{HF}}$ and the SAPT Components Included in Equation (8) at and Around Geometry G1 as a Function of R	26	
5a. The Interaction Energy and Individual Components Indicated in Equation (9) Are Shown in Histogram Format to Illustrate the Relative Importance of the Various Energy Contributions at the G1, G2, G3, and G4 Minima	28	
5b. A Histogram Is Shown Containing $E_{\text{int}}^{\text{HF}}$ and the SAPT Components Included in Equation (8) at the G1, G2, G3, and G4 Minima	29	
6. $E_{\text{int}}^{(+\text{mb})}$ as a Function of β_1 Is Shown for $R = 4.0$ and $R = 4.75 \text{ \AA}$, With the Remaining Coordinates Taken From G1	33	
7a. The Interaction Energy $E_{\text{int}}^{(+\text{mb})}$ and Its Components According to Equation (9) Shown as a Function of β_1 for $R = 4.0 \text{ \AA}$	34	
7b. The HF Interaction Energy $E_{\text{int}}^{\text{HF}}$ and Its Components According to Equation (8) Shown as a Function of β_1 for $R = 4.0 \text{ \AA}$	35	
8a. The Interaction Energy $E_{\text{int}}^{(+\text{mb})}$ and Its Components According to Equation (9) Shown as a Function of β_1 for $R = 4.75 \text{ \AA}$	36	
8b. The HF Interaction Energy $E_{\text{int}}^{\text{HF}}$ and Its Components According to Equation (8) Shown as a Function of β_1 for $R = 4.75 \text{ \AA}$	37	

INTENTIONALLY LEFT BLANK.

List of Tables

<u>Table</u>	<u>Page</u>
1. Nuclear Coordinates in Å for the CH ₃ CN Monomer Geometry	6
2. The Coordinates for the Local Minimum Geometries G1, G2, G3, and G4	8
3. Comparison of the SAPT Interaction Energy Components for the CH ₃ CN-CO ₂ Interaction Using a MC+BS and the Analogous DCBS at the Two Local Minimum Geometries G1 and G4	15
4. Comparison of SM Results With SAPT Results at Three Local Minimum Geometries	16
5. Contribution of Basis Functions of Different Angular Symmetry Placed at the Midbond Position to the $E_{\text{disp}}^{(20)}$ Energy in kcal/mol	18
6. Potential Cuts in R Through the Two Local Minimum Geometries G1 and G2 ...	20
7. Potential Cuts in R Through the Local Minimum Geometry G3	22
8. Potential Cuts in R Through the Local Minimum Geometry G4	23
9. Potential Cuts in β_1 at Geometry G1 for Two Different R Values	31
10. Potential Cuts in β_1 at Geometry G1 for $R = 4.75$ Å	32
A-1. The Supplementary Tables Complement Tables 6–10 and Provide a Complete Description of All Single-Point Symmetry-Adapter Perturbation Theory (SAPT) Computations Used in the Present Work	47
A-2. Supplementary Tables Continued	49
A-3. Supplementary Tables Continued	51
A-4. Supplementary Tables Continued	53
A-5. Supplementary Tables Continued	55

<u>Table</u>		<u>Page</u>
A-6.	Supplementary Tables Continued	57
A-7.	Supplementary Tables Continued	59
A-8.	Supplementary Tables Continued	61
A-9.	Supplementary Tables Continued	63
A-10.	Supplementary Tables Continued	65
A-11.	Supplementary Tables Continued	67
A-12.	Supplementary Tables Continued	69
A-13.	Supplementary Tables Continued	71
A-14.	Supplementary Tables Continued	73
A-15.	Supplementary Tables Continued	75

1. Introduction

Weak intermolecular interactions play a particularly important role in the computer simulation of liquids [1]. An excellent example of a process which displays this characteristic is supercritical fluid (SCF) CO₂ extraction [2]. When SCFs are compressed to liquid-like densities, their solvent strength dramatically increases. A closed system can then be built to extract materials of interest from a more general mixture. Carbon dioxide (CO₂) proves to be an excellent choice for this process because of both its nondestructive character and because it is environmentally benign. Some industrial processes, such as caffeine extraction, already make profitable use of this procedure.

The Department of Defense (DOD) community sets a priority on developing an environmentally beneficial and cost-effective way to recycle solid energetic materials which have reached the end of their rated lifetime. Significant environmental and economic advantages could result from an industrial scale, closed-system recycling procedure based on supercritical CO₂ for this particular application. Unfortunately, certain components in composite propellants are not sufficiently soluble in pure SCF CO₂ to make this extraction process viable. The solubility characteristics of these components can be enhanced with the addition of so-called modifier molecules. These typically polar molecules increase the solubility strength of the SCF, but little is known about the detailed molecular interactions accounting for the increased solubility. The first step towards simulating the entire system is knowledge of accurate intermolecular potentials for all dimer interactions in the system—the solvent-solute, solvent-modifier, modifier-solute, and each with itself (e.g., solvent-solvent). Methyl cyanide (CH₃CN) has been shown to be an effective polar modifier for enhancing the dissolution of one of the important solid energetic materials, cyclotrimethylenetrinitramine (RDX), in SCF CO₂ [3]. This work will focus on mapping the detailed potential energy surface (PES) of CO₂ interacting with CH₃CN.

Symmetry-Adapted Perturbation Theory (SAPT) [4, 5] is a natural choice to find the interaction energy of the CH₃CN-CO₂ system or any two closed-shell weakly interacting atomic or molecular systems. SAPT *directly* and naturally separates the interaction energy into four physically

interpretable components: (1) electrostatics, (2) exchange, (3) dispersion, and (4) induction. Each component has distinct radial and angular dependence for each system and can be fitted to an analytical form independently of the other components. This can lead to significant physical insight about the interaction in contrast to the currently more popular supermolecular (SM) method which returns *only* a single number. SAPT has been used to successfully investigate a variety of systems including Ar-H₂ [6], He-HF [7], He-CO [8], Ar-HF [9], He-C₂H₂ [10], H₂-CO [11], and (H₂O)₂ [12].

Section 2 introduces definitions necessary for analyzing SAPT results. Section 3 describes the computational details. Section 4 investigates some representative cuts of the PES for the CH₃CN-CO₂ system and specifies the coarse grid used for the majority of the geometrical configurations investigated. Section 5 presents conclusions.

2. Method

Jeziorski, Moszynski, and Szalewicz [4] and Szalewicz and Jeziorski [5] present recent reviews of SAPT and provide an excellent overview of the method. Further details on the explicit derivation of the theory and implementation can be found in section 6 [13–20]. We present only a necessary amount of notation to interpret the results of the present work.

The dimer Hamiltonian is decomposed by SAPT into three general parts. The first two, the Fock operator F , and the Møller-Plesset-type intramonomer correlation operator W , have separate contributions from both systems A and B and are written as $F = F_A + F_B$ and $W = W_A + W_B$, respectively. The third part of the Hamiltonian is the intermolecular interaction operator V which mediates interactions between the two systems. The total Hamiltonian is then written as $H = F + V + W$. The wave function used with this Hamiltonian is the product of the system A and B wave functions. This product wave function does not obey the Pauli principle. The correct permutational symmetry of the electrons between systems is imposed on the product wave functions using an antisymmetrizer described in more detail in Jeziorski, Moszynski, and Szalewicz [4] and Szalewicz and Jeziorski [5].

The intermolecular interaction energy E_{int} within the SAPT framework can then be expanded in powers of the intermolecular interaction operator V as

$$E_{\text{int}} = E_{\text{elst}}^{(1)} + E_{\text{exch}}^{(1)} + E_{\text{pol}}^{(2)} + E_{\text{exch}}^{(2)} + \dots, \quad (1)$$

where the first two terms on the right-hand side of equation (1) can be interpreted as the classical electrostatic (coulomb) and exchange energies, respectively. The exchange components are the result of the antisymmetrization previously mentioned. They can also be viewed as an effect of resonance tunneling of electrons between the interacting systems.

The second-order terms in equation (1) naturally separate into dispersion and induction components as

$$E_{\text{pol}}^{(2)} = E_{\text{ind}}^{(2)} + E_{\text{disp}}^{(2)} \quad (2)$$

and analogously for the exchange component

$$E_{\text{exch}}^{(2)} = E_{\text{exch-ind}}^{(2)} + E_{\text{exch-disp}}^{(2)}. \quad (3)$$

The dispersion energy is a result of the interactions of the two monomers' instantaneous electric moments. The induction energy describes the interactions of the permanent and induced multipole moments of the two monomers. The second-order exchange-dispersion and exchange-induction energies result from electron tunneling between systems related to the dispersion and induction components of the wave function.

Equation (1) implicitly indicates the inclusion of full *intramonomer* electron correlation. Within the SAPT framework, this is only currently possible in the case of four-electron systems [21, 22]. To describe the intramonomer electron correlation for larger systems, we also perturbationally

expand each of the components in equation (1) in powers of W . For example, the first-order polarization energy is now expanded in a double perturbation series as

$$E_{\text{elst}}^{(1)} = \sum_{k=0}^{\infty} E_{\text{elst}}^{(1k)}, \quad (4)$$

where k indicates the order in W . It is convenient to split expansions like equation (4) into terms which include and neglect intramonomer correlation. This is written explicitly for the first-order polarization energy as

$$E_{\text{elst}}^{(1)} = E_{\text{elst}}^{(10)} + \epsilon_{\text{elst}}^{(1)}, \quad (5)$$

where the second term sums all terms of order one and above in W in equation (4). The sum of these terms through the k th order in W will be indicated by the notation $\epsilon_{\text{elst}}^{(1)}(k)$. Similar definitions are assumed for the other components as well.

The first-order polarization and second-order induction components are calculated with the inclusion of the coupled Hartree-Fock (HF)-type response of a perturbed system. Components computed in this manner will be indicated with the subscript "resp" as in $E_{\text{ind},\text{resp}}^{(20)}$. The intramonomer correlation effects in induction interactions will be approximated by $'E_{\text{ind}}^{(22)}$, the so-called "true" correlation contribution which collects those parts of the $E_{\text{ind}}^{(22)}$ correction that are not included in $E_{\text{ind},\text{resp}}^{(20)}$. Note that $E_{\text{elst}}^{(10)} = E_{\text{elst},\text{resp}}^{(10)}$.

The correlated SAPT portion of the interaction energy then includes

$$E_{\text{int}}^{\text{corr}} = \epsilon_{\text{elst},\text{resp}}^{(1)} (3) + \epsilon_{\text{exch}}^{(1)} (2) + 'E_{\text{ind}}^{(22)} + E_{\text{disp}}^{(20)} + \epsilon_{\text{disp}}^{(2)} (2) + E_{\text{exch-disp}}^{(20)} + 'E_{\text{exch-ind}}^{(22)}. \quad (6)$$

The ' $E_{\text{exch-ind}}^{(22)}$ ' component which partially quenches the corresponding induction component is not currently coded. We have estimated it by scaling $E_{\text{exch-ind}}^{(20)}$ by the ratio of the correlated to uncorrelated induction components by

$$E_{\text{exch-ind}}^{(22)} \approx E_{\text{exch-ind,resp}}^{(20)} \frac{E_{\text{ind}}^{(22)}}{E_{\text{ind,resp}}^{(20)}}. \quad (7)$$

There exists the following relation between the SM HF interaction energy and the SAPT expansion [23, 24]:

$$E_{\text{int}}^{\text{HF}} = E_{\text{elst}}^{(10)} + E_{\text{exch}}^{(10)} + E_{\text{ind,resp}}^{(20)} + E_{\text{exch-ind,resp}}^{(20)} + \delta^{\text{HF}}, \quad (8)$$

where δ^{HF} indicates the sum of higher order induction and exchange terms. The first- and second-order terms in equation (8) are those calculated in the current implementation of SAPT. δ^{HF} is defined as the difference between the sum of these SAPT terms and the supermolecule HF energy, $E_{\text{int}}^{\text{HF}}$.

In order to include some of the higher order induction terms currently not available in SAPT, we use a hybrid method which includes the SM HF energy and the correlated portion of the SAPT components indicated in equation (6). The total interaction energy in the present work will then be approximated by combining equation (6) and equation (8) to give

$$E_{\text{int}} = E_{\text{int}}^{\text{HF}} + E_{\text{int}}^{\text{corr}}. \quad (9)$$

For more discussion about this relationship and further references, see Szalewicz and Jeziorski [5]. The Boys-Bernardi [25] counterpoise (CP) scheme is always used to compute $E_{\text{int}}^{\text{HF}}$ and other SM quantities of interest in order to eliminate basis set superposition error (BSSE) [5, 26].

3. Computational Details

We used Dunning's correlation-consistent basis augmented with diffuse functions labeled aug-cc-PVDZ [27–29] as a starting point for all calculations with modifications. The CH₃CN monomer geometry was determined by a QCISD [30–32] calculation with the full inclusion of inner shell electrons optimizing the monomer's total energy. The nuclear coordinates for this monomer are presented in Table 1. For carbon dioxide, a carbon-oxygen distance of 1.162047 Å was taken from Sadleg, Szczesniak, and Chalasinski [33]. Both monomer geometries were then fixed for all further study. Gaussian 94 [34] and Atmol [35] were both used to perform the necessary SCF calculations. Both programs are interfaced to the SAPT suite of codes [36].

Table 1. Nuclear Coordinates in Å for the CH₃CN Monomer Geometry. Each HCCN Angle Is 109.731504°. The Center of Mass for the System is 0.68927 Å From the Inner Carbon Between the Two Carbon Atoms.

Atom	x	y	z
C	0.0	0.0	0.0
C	1.477947	0.0	0.0
N	-1.170898	0.0	0.0
H	1.849295	0.0	1.0353445
H	1.849295	-0.896636	-0.517673
H	1.849295	-0.896636	-0.517673

Optimizations of the full dimer energy in the full dimer basis set with fixed internal monomer geometries were then performed at the MP2 level of theory again with full inclusion of inner core electrons. Four local minimum geometries were located with this procedure and will be designated G_n, n = 1, 2, 3, or 4. These geometries, shown in Figure 1, serve as starting points for investigating interesting portions of the PES. Since a CP-corrected optimization procedure was not used for the minimizations, BSSE may affect the positions of the local minima. No attempt to quantify this error was made since the minimum geometries were used only for the purpose previously mentioned.

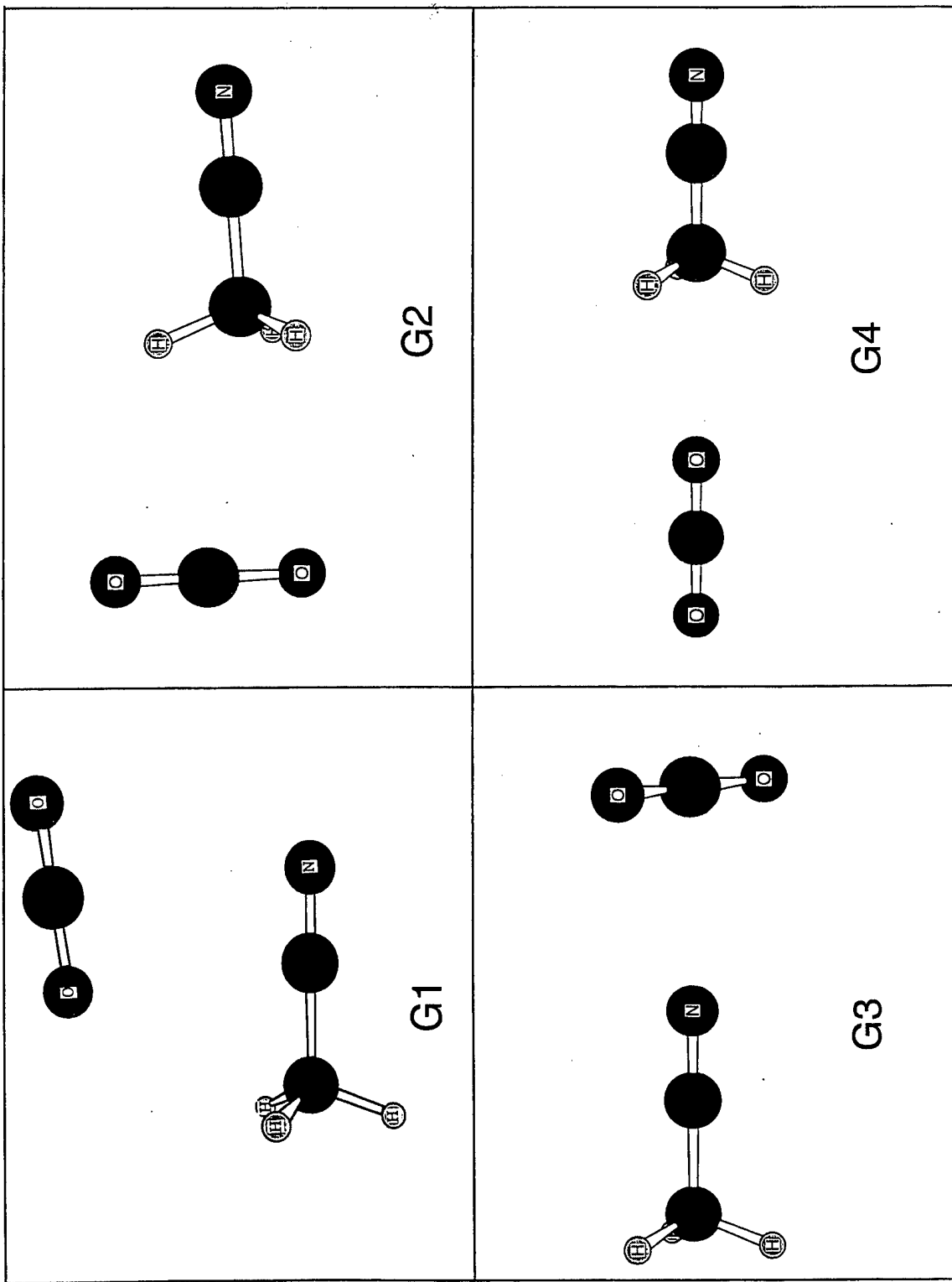


Figure 1. The Four Local Minimum Geometries Labeled as G1, G2, G3, and G4 in Table 2. The Geometry G1 is the Most Strongly Bound of These Four Minima at -2.90 kcal/mol .

Subsequent discussion of these geometries refers to the SAPT computations which are not biased by BSSE.

The coordinates of the MP2 local minimum geometries are provided in Table 2. A description of the coordinate system is given in the next paragraph. In configuration G1, the CO₂ axis is in a slipped, nearly parallel position (away from the CH₃ group) with respect to the C₃ axis of the CH₃CN molecule (see Figure 1). In configuration G2, the CO₂ is oriented along and nearly perpendicular to the major axis of CH₃CN toward the CH₃ group. Configuration G4 has the CO₂ in a similar location, but the CO₂ major axis is nearly aligned with the CH₃CN axis. Finally, configuration G3 is oriented in the same way as G2 except toward the nitrogen atom.

Table 2. The Coordinates for the Local Minimum Geometries G1, G2, G3, and G4 (The Units for Distance and Angles Are Å and Degrees, Respectively.)

Geometry	R	β_1	γ_1	β_2	α_2
G1	3.327156	107.746148	119.852998	116.669519	359.978866
G2	4.652572	7.954955	59.997536	95.612989	359.870681
G3	4.276012	179.643584	60.183120	89.771324	170.272920
G4	5.572889	0.012626	61.490949	179.921826	1.518053

The dimer configuration has been specified by coordinates consisting of a separation distance R and two sets of Euler angles as given in Brink and Satchler [37]. A pictorial representation of these coordinates as applied to this system can be seen in Figure 2. R is defined as the length of the vector connecting the centers of mass between the two monomers. Each center of mass is located at the origin of a system of Cartesian coordinate axes, and these two sets of axes remain fixed and parallel to the space-fixed coordinate system. The vector R coincides with the Z axis and points in the positive Z direction. One set of Euler angles is assigned to each of the molecules and is defined with respect to the Cartesian coordinate axes associated with that molecule. The angles are given by the variables ($\alpha_1, \beta_1, \gamma_1$) for the orientation of CH₃CN, and ($\alpha_2, \beta_2, \gamma_2$) for CO₂.

The dimer configurations are obtained from the independent Euler angles by rotating CH₃CN about γ_1 , followed by rotating each monomer through its respective β_1 angle, and finally rotating the CO₂ molecular axis through its α_2 angle. γ_1 is the angle of rotation of CH₃CN about its C₃ axis (hereafter referred to as its “molecular axis”). This can be further defined as a rotation about the CCN molecular axis between a half plane and the stationary XZ plane. The half-plane is formed by the CH₃CN molecular axis and one of the CH bonds. γ_1 is taken to be zero when the half-plane containing the CH bond coincides with the XZ plane and lies in the positive X hemisphere (see Figure 2). γ_1 is then allowed to vary between 0 and 120°, with the sense of rotation always being done such that the CH bond lies in the positive Y hemisphere. With this definition of γ_1 , one can take advantage of the C_{3v} symmetry of CH₃CN. γ_2 would be the angle of rotation for CO₂ about its molecular axis, but due to its cylindrical symmetry, it is undefined and allows us to reduce the coordinates from six independent coordinates to five.

β_1 is the simple angle between the positive Z axis and the vector drawn from the COM of CH₃CN to the methyl carbon. Likewise, β_2 is the angle between one of the CO bonds and the part of the Z axis where Z > R. Both β_1 and β_2 are allowed to vary from 0 to 180°. α_2 is an angle of rotation between two half planes, both of which have their edge coincidental with the Z axis. The first half plane, which is taken to remain stationary, is formed by the Z axis and the positive X axis. The second half plane (i.e., the rotating plane) is formed by the Z axis and the CO bond involved in the definition of β_2 . α_2 can vary from 0 to 360°, but is zero when the half plane containing the CO is coincidental with the XZ plane and pointing in the +X direction. The sense of rotation is clockwise when viewed down the Z axis from -Z to +Z. The final Euler angle, α_1 , would rotate the molecular axis for CH₃CN out of the XZ plane. This corresponds to the rotation of the entire dimer system, in a fixed configuration, about the Z axis. Thus, α_1 is not involved in the definition of the relative positions of the two molecules, and thus can be fixed to zero. The results of this are that the CCN molecular axis always lies in the XZ plane, and the β_1 angle always lies in the positive X direction.

There are a few symmetries within this system which can be exploited to reduce the total number of grid points that need to be considered. The linearity of the CO₂ molecule eliminates the need to

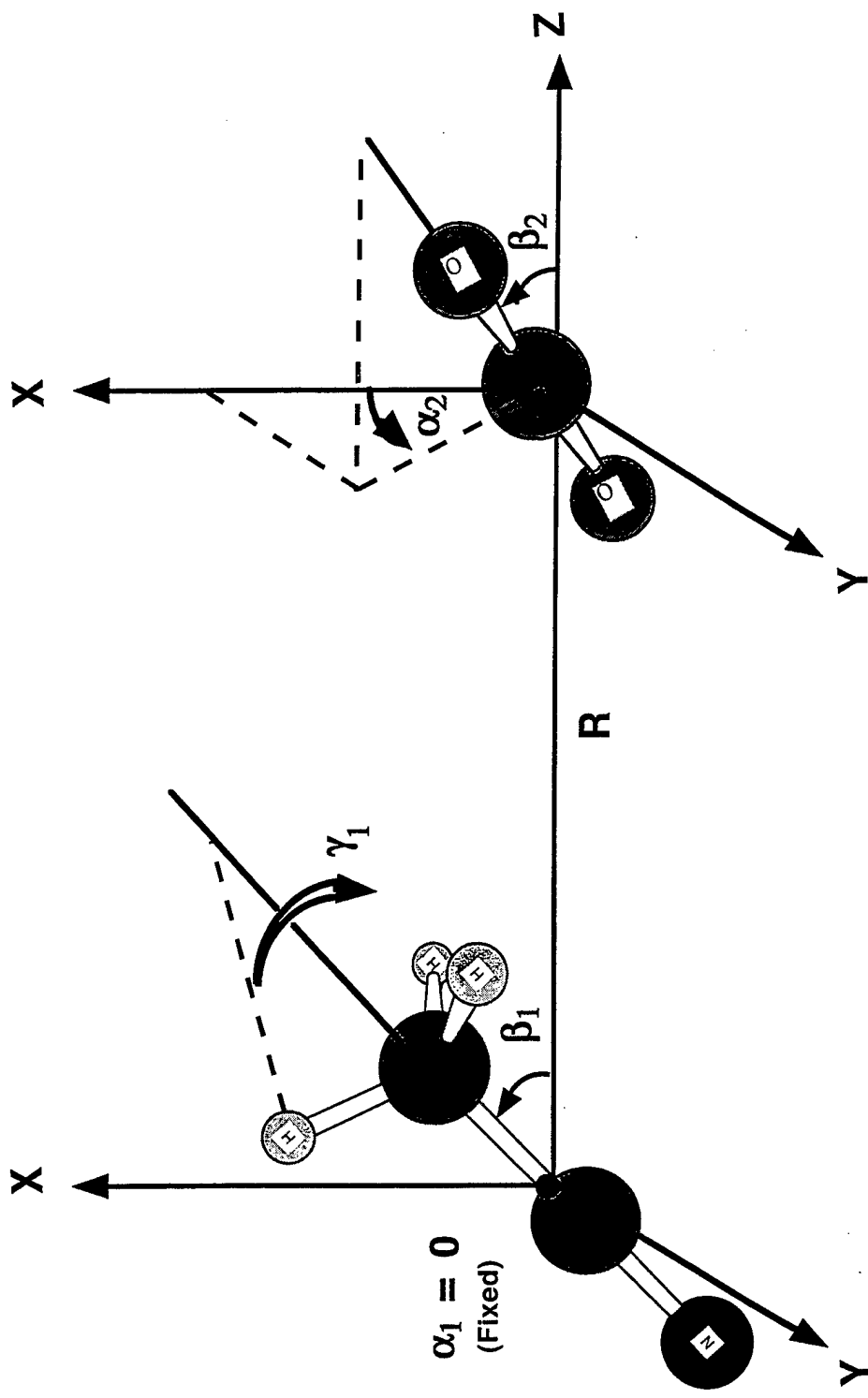


Figure 2. Graphical Representation of the Coordinate System Used to Specify the Dimer Configuration. The Vector R Is Coincidental With the Z Axis and Connects the Centers of Mass of the Two Dimers. Associated With Each Monomer Is a Set of Euler Angles as Given in Brink and Satchler [37]. The Orientation of CH_3CN Is Given by the Angles α_1 , β_1 , and γ_1 , Where α_1 Is Held Fixed at 0, and the Orientation of CO_2 Is Given by α_2 and β_2 . Due to the Cylindrical Symmetry of CO_2 , γ_2 Is Undefined, Which Reduces the Number of Independent Variables to 5. (See the Text for Further Explanation.)

consider the sixth coordinate necessary for describing general rigid two-body interactions. Describing E_{int} as a potential function of five coordinates by

$$E_{\text{int}} = V(R, \beta_1, \gamma_1, \beta_2, \alpha_2), \quad (10)$$

the symmetries can be concisely written as

$$V(R, \beta_1, \gamma_1, \beta_2, \alpha_2) = V(R, \beta_1, \gamma_1 + \frac{2n\pi}{3}, \beta_2, \alpha_2) : n = 1, 2, \quad (11)$$

$$V(R, \beta_1, \gamma_1, \beta_2, \alpha_2) = V(R, \beta_1, -\gamma_1, \beta_2 - \alpha_2), \quad (12)$$

$$V(R, \beta_1, \gamma_1, \beta_2, \alpha_2) = V(R, \beta_1, \gamma_1, \pi - \beta_2, \pi + \alpha_2), \text{ and} \quad (13)$$

$$V(R, \beta_1, \gamma_1, \beta_2, \alpha_2) = V(R, \beta_1, -\gamma_1, \pi - \beta_2, \pi - \alpha_2); \quad (14)$$

further symmetries in special cases can be written as

$$V(R, \beta_1, \gamma_1, 0, \alpha_2) = V(R, \beta_1, \gamma_1, 0, 0), \quad (15)$$

$$V(R, 0, \gamma_1, \beta_2, \alpha_2) = V(R, 0, 0, \beta_2, \alpha_2 - \gamma_1), \quad (16)$$

$$V(R, \pi, \gamma_1, \beta_2, \alpha_2) = V(R, \pi, 0, \beta_2, \alpha_2 + \gamma_1), \quad (17)$$

$$V(R, 0, \gamma_1, 0, \alpha_2) = V(R, 0, 0, 0, 0), \text{ and} \quad (18)$$

$$V(R, \pi, \gamma_1, 0, \alpha_2) = V(R, \pi, 0, 0, 0). \quad (19)$$

Including these symmetry constraints significantly reduced the total number of points needed for our coarse grid covering of the total PES.

A total of 187 points on the PES were computed for various combinations of R , β_1 , γ_1 , β_2 , and α_2 . The first group of points chosen was based on the four geometries presented in Table 2. For each of these geometries, we varied only the R coordinate and computed enough points to show the depth and shape of the local minimum well. This required 27 points total for all four geometries investigated, and the results are shown in Tables 6–8. Next, we covered a coarse grid in R , β_1 , and γ_1 while fixing the remaining coordinates to those of geometry G1. For this collection of points, we selected values for R from the set (G1, 3.5, 3.75, 4.0, 4.25, 4.5, 4.75 Å). For β_1 , we selected from the set (0, 45, 90, 135, 180°) and for γ_1 , either the G1 value or G1 + 60°. A subset of these points, where only R and β_1 vary, is given in Tables 9 and 10 for the purpose of discussion, and the remainder of the data points are included in Tables A12–A15 in the appendix. A clarification is required concerning the coordinates for the points in Tables A12–A15. For these four tables, the algorithm written to transform from internal coordinates to Cartesian coordinates (used as input to the SAPT procedure) unintentionally caused a reflection through the XZ plane of the γ_1 value in structure G1. This generated G1-like structures that differ from G1 by only +0.294° in the γ_1 torsion angle. Accordingly, the starting γ_1 value used in Tables A12–A15 is not 119.853°, but rather 119.853° + 0.294°, or taking into account the C_{3v} axis, $\gamma_1 = +0.147^\circ$. The coordinates in Tables A12–A15 include this difference in γ_1 . Finally, we selected a coarse grid covering the entire PES with values for $R = (3, 4, 5, 6 \text{ \AA})$, $\beta_1 = (0, 45, 90, 135, 180^\circ)$, $\gamma_1 = (0, 60^\circ)$, $\beta_2 = (0, 45^\circ)$, and $\alpha_2 = (0, 45, 90^\circ)$.

Since SAPT interaction energies are rigorously free of BSSE, there is no *a priori* need to compute the SAPT components in a dimer-centered basis set (DCBS) as is necessary in the SM CP-corrected approach. Williams et al. [38] investigated some alternate schemes for the placement of basis functions for efficient computation of SAPT components, called monomer-centered and monomer-centered plus basis sets (MCBS and MC+BS), respectively. In a “pure” MCBS, each monomer uses only those basis functions that are placed on its own nuclear centers. The “plus” in the MC+BS case indicates basis functions used in addition to the monomers’ original basis set.

The location for these additional functions in the MC+BS are the original locations of the basis functions on the ghost monomer. Eventually, adding functions to the MCBS in this manner would produce the full DCBS. The goal, however, is to reduce the computational effort below that required for the full DCBS while retaining acceptable accuracy. A MC+BS that best balances the goals of computational tractability and accuracy in SAPT calculations is one in which only the valence basis functions are retained on the ghost monomer. Explicitly, when a CH₃CN, SAPT computation is being performed, only *s*- and *p*-type functions are included in the CO₂ ghost basis set. Likewise, when the CO₂ computation is being performed, only *s* and *p* functions are placed on the C or N atoms of CH₃CN, and only *s*-type functions are placed on the H atoms. This arrangement allows a 20–30% reduction in the size of the basis compared to the equivalent DCBS, with almost no sacrifice in accuracy. This significantly reduces the computational effort because the most computationally expensive SAPT component, $E_{\text{disp}}^{(22)}$, scales as $n_o^3 n_v^4$ where n_o^3 and n_v^4 are the numbers of occupied and virtual orbitals, respectively. In this manner, the full DCBS size of 165 basis functions was reduced to a MC+BS size of 135 and 117 basis functions for monomer CH₃CN and CO₂, respectively.

A separate computation was performed for the $E_{\text{disp}}^{(20)}$ component, which is variational in character. The MC+BS was augmented with a large midbond set of 2s2p2d1f1g placed at the midpoint of the line segment defining the coordinate *R*. The orbital exponents are 0.15 and 0.6 for *s*, *p*, and *d* functions and 0.3 for the *f* and *g* functions. These functions were selected by optimizing one basis function of each type to one digit accuracy with the goal of maximizing the absolute value of the $E_{\text{disp}}^{(20)}$ energy. The *s*, *p*, and *d* functions were then each split into two basis functions using the “even scaling rule” [39] producing the orbital exponents given previously. This new value for $E_{\text{disp}}^{(20)}$ was then used in place of the one which was computed using the basis set described in the previous paragraph. The addition of midbond functions for this component will be indicated with a superscript “(+mb)” for both the leading term in the second-order dispersion energy and for the total interaction energy as $E_{\text{disp}}^{(20)(+\text{mb})}$ and $E_{\text{int}}^{(+\text{mb})}$, respectively.

4. Results and Discussion

To check the quality of the atomic orbital (AO) basis set used on the monomers, we report the calculated electric dipole and quadrupole moment of CO₂ and CH₃CN, respectively. The theoretical values are calculated at the QCISD level with the aug-cc-pvdz basis set used on the monomers throughout this work. The electric dipole moment of CH₃CN is predicted to be 3.95 debye, while experimenting gives 3.92 debye [41]. Values for the CO₂ experimental quadrupole moment [42–45] vary between –1.34 and 1.5 × 10^{–19} coulomb Å², while the calculated value lies at the upper end of this range with a value of –1.514 × 10^{–19} coulomb Å².

Table 3 compares the SAPT components computed using the MC+BS described in section 3 with the equivalent DCBS at the two geometries G1 and G4. The difference in the first-order components between a MC+BS and the equivalent DCBS is less than about 0.01 kcal/mol. Aside from $E_{\text{disp}}^{(20)}$, which will be replaced as previously described, the second-order components differ by no more than 0.04 kcal/mol. Further, the second-order differences at least partially offset each other for the geometries shown, though this cannot be relied upon over the entire PES. This level of error should be substantially smaller than other sources of error in the present work. Further, the reduction in the number of basis functions decreases the computational cost at each geometrical configuration by more than a factor of three. For the most time-consuming component, the triples portion of $E_{\text{disp}}^{(22)}$, this cost is cut by 3.5 times by using a MC+BS rather than a DCBS.

Table 3 further shows that the largest components in absolute magnitude for G1 and G4 are $E_{\text{elst}}^{(10)}$, $E_{\text{exch}}^{(10)}$, and $E_{\text{disp}}^{(20)}$. Previous experience [38] and Table 3 indicate that the first two components converge very quickly with basis set and are sufficiently converged with the current MC+BS. More attention must be paid to $E_{\text{disp}}^{(20)}$ since small percentage errors in this component can translate into relatively large absolute errors in the final energies. With this in mind, the convergence properties of this component with respect to basis set saturation will be studied in more detail later.

Table 3. Comparison of the SAPT Interaction Energy Components for the CH₃CN-CO₂ Interaction Using a MC+BS and the Analogous DCBS at the Two Local Minimum Geometries G1 and G4 (The Units for the Energies Are kcal/mol.)

Geometry Basis Type	G1		G4	
	MC+BS	DCBS	MC+BS	DCBS
$E_{\text{elst}}^{(10)}$	-3.64	-3.64	-1.08	-1.07
$\varepsilon_{\text{elst,resp}}^{(1)}(3)$	0.53	0.53	0.11	0.11
$E_{\text{exch}}^{(10)}$	3.88	3.88	1.09	1.09
$\varepsilon_{\text{exch}}^{(1)}(2)$	0.25	0.26	0.20	0.21
$E_{\text{disp}}^{(20)}$	-3.07	-3.22	-1.21	-1.26
$\varepsilon_{\text{disp}}^{(2)}(2)$	-0.03	-0.05	-0.08	-0.10
$E_{\text{disp}}^{(2)}$	-3.09	-3.28	-1.30	-1.36
$E_{\text{ind,resp}}^{(20)}$	-2.01	-2.05	-0.26	-0.26
$E_{\text{ind}}^{(22)}$	0.05	0.05	-0.03	-0.03
$E_{\text{exch-disp}}^{(20)}$	0.32	0.36	0.07	0.08
$E_{\text{exch-ind,resp}}^{(20)}$	1.57	1.57	0.15	0.15
$E_{\text{int}}^{\text{a}}$	-2.38	-2.51	-1.06	-1.12

^a Computed according to equation (9).

Table 4 compares the best currently coded SAPT approximation to each SM energy (HF, MP2, MP3, and MP4), with the appropriate sums detailed in the footnotes to this table. At the G1 geometry δ^{HF} , the difference between the four-term SAPT approximation to $E_{\text{int}}^{\text{HF}}$ and $E_{\text{int}}^{\text{HF}}$ itself is less than 0.2 kcal/mol. While this is a small difference in absolute magnitude, it represents a large percentage of $E_{\text{int}}^{\text{HF}}$. This large percentage is misleading, though, since it occurs near the point where $E_{\text{int}}^{\text{HF}}$

Table 4. Comparison of SM Results With SAPT Results at Three Local Minimum Geometries (The SM Iteration Energies Are Computed Using the Boys-Bernardi [25] CP Scheme; the SAPT Components Use a MC+BS. The DCBS Values Available for Geometries G1 and G4 Are Displayed in the Footnotes if They Differ by More Than 0.02 kcal/mol From the MC+BS Value.)

Geometry Basis Type	G1	G2	G4
$E_{\text{int}}^{\text{HF}}$	-0.39	1.30	-0.15
$E_{\text{SAPT}}^{\text{HF}} \text{ a}$	-0.21	1.36	-0.10
δ^{HF}	-0.18	-0.06	-0.06
$E_{\text{int}}^{\text{MP2}}$	-1.75	-1.49	-0.75
$E_{\text{SAPT}}^{\text{MP2}} \text{ b}$	-1.73 ^c	-1.52	-0.80 ^d
δ^{MP2}	-0.03	0.05	0.05
$E_{\text{int}}^{\text{MP3}}$	0.47	0.23	0.09
$E_{\text{SAPT}}^{\text{MP3}} \text{ e}$	0.56	0.30	0.17
δ^{MP3}	-0.08	-0.07	-0.08
$E_{\text{int}}^{\text{MP4}}$	-0.50	-0.30	-0.16
$E_{\text{SAPT}}^{\text{MP4}} \text{ f}$	-0.81 ^g	-0.30	-0.29
δ^{MP4}	0.30	0.00	0.13
$E_{\text{int}}^{(\text{HF} + \text{MP2} + \text{MP3} + \text{MP4})}$	-2.17	-0.26	-0.97
$E_{\text{SAPT}}^{\text{h}}$	-2.37	-0.22	-1.07
$\delta^{(\text{HF} + \text{MP2} + \text{MP3} + \text{MP4})}$	0.20	-0.04	0.10

^a $E_{\text{SAPT}}^{\text{HF}} = E_{\text{elst}}^{(10)} + E_{\text{exch}}^{(10)} + E_{\text{ind, resp}}^{(20)} + E_{\text{exch-ind, resp}}^{(20)}$.

^b $E_{\text{SAPT}}^{\text{MP2}} = E_{\text{disp}}^{(20)} + E_{\text{elst, resp}}^{(12)} + 'E_{\text{ind, resp}}^{(22)} + \varepsilon_{\text{exch}}^{(1)}(2) + E_{\text{exch-disp}}^{(20)} + 'E_{\text{exch-ind}}^{(22)}$.

^c DCBS value is -1.84 kcal/mol.

^d DCBS value is -0.84 kcal/mol.

^e $E_{\text{SAPT}}^{\text{MP3}} \approx E_{\text{elst, resp}}^{(13)} + E_{\text{disp}}^{(21)}$.

^f $E_{\text{SAPT}}^{\text{MP4}} \approx E_{\text{disp}}^{(22)}$.

^g DCBS value is -0.83 kcal/mol.

^h Computed according to equation (9).

crosses zero. The absolute values of $E_{\text{pol}}^{(10)}$ and $E_{\text{exch}}^{(10)}$ given in Table 3 are nearly 4 kcal/mol at G1, but are opposite in sign and cancel to within a fraction of a kcal/mol. The comparison to SM-MP2 is quite good at all three geometries, probably indicating reasonably good agreement over the entire PES. The SM-MP3 energies show a small difference in absolute values of less than 0.1 kcal/mol. The SM-MP4 energy comparison shows the largest deviation of 0.3 kcal/mol from the SAPT approximation at geometry G1. This deviation is probably due to accumulation of errors resulting from the neglect of $E_{\text{elst,resp}}^{(14)}$ and $E_{\text{exch-disp}}^{(22)}$.

Table 5 investigates the effect on $E_{\text{disp}}^{(20)}$ of adding basis functions with different angular symmetries placed at the midbond position as described in section 3. The value for this component using the DCBS from Table 3 is repeated in Table 5 for comparison. The addition of the full midbond $2s2p2d1f1g$ set lowers this energy component by 0.53 (17%) and 0.18 (15%) kcal/mol for the geometries G1 and G4, respectively, from its MC+BS value. This results in a 22% and 16% lowering of the final value of E_{int} for these geometries. By adding only s and p functions at the midbond, the value of $E_{\text{disp}}^{(20)}$ is already lower than the corresponding DCBS value while using 22 fewer basis functions. This indicates that midbond functions are helping to converge this component faster than nuclear-centered basis functions of higher angular symmetry placed at the other nuclear centers. The increase in the computational cost of treating only $E_{\text{disp}}^{(20)}$ with the full set of midbond basis functions is rather minor, yet provides a significant increase in accuracy for this component. Using this set of midbond functions in the computation of all SAPT components would not have improved the accuracy of the results in proportion to the amount of additional computer time needed.

Figure 3 displays a cut in R for each of the four geometries, G1, G2, G3, and G4. Tables 6, 7, and 8 provide the individual SAPT components and total interaction energy for each of the points shown in Figure 3. Geometry G1, with CO₂ roughly parallel to the CCN axis, has a total interaction

Table 5. Contribution of Basis Functions of Different Angular Symmetry Placed at the Midbond Position to the $E_{\text{disp}}^{(20)}$ Energy in kcal/mol (The Table Indicates the Successive Inclusion of Each of the Symmetries, e.g., Row g Includes the Full $2s2p2d1f1g$ Set. The Numerical Values of the Exponents Used for Each Symmetry Are Found in Section 3. The Number of Basis Functions Refers to the CH_3CN Monomer Including Midbond Functions and Ghost Functions Placed on the CO_2 Nuclear Centers. The Values Computed Without Midbond Functions Are Taken From Table 3.)

Basis Type	Midbond		Basis Size	Geometry	
	Number	Symmetry		G1	G4
DCBS	—	—	165	-3.22	-1.26
MC+BS	—	—	135	-3.07	-1.21
MC+BS	2	—	<i>s</i>	-3.17	-1.23
MC+BS	2	—	<i>p</i>	-3.35	-1.31
MC+BS	2	—	<i>d</i>	-3.47	-1.36
MC+BS	1	—	<i>f</i>	-3.55	-1.38
MC+BS	1	—	<i>g</i>	-3.60	-1.39

energy of $E_{\text{int}}^{(+\text{mb})} = -2.90$ kcal/mol. This is slightly more stable than G3, where $E_{\text{int}}^{(+\text{mb})} = -2.82$ kcal/mol, and the CO_2 is perpendicular to the CCN axis. The interaction energy of -1.25 kcal/mol at geometry G4 is significantly smaller in magnitude than for the former two geometries. Finally, geometry G2 is only weakly bound at -0.43 kcal/mol.

Figure 4a shows the cut through geometry G1 broken into the components indicated in equation (9). The minimum energy for $E_{\text{int}}^{\text{HF}}$ is near $R = 3.75 \text{ \AA}$, while the full interaction energy, including correlation corrections, predicts the minimum to occur near $R = 3.33 \text{ \AA}$ or 0.4 \AA shorter than the HF value. This comparison clearly indicates the need to include the intermolecular electron correlation effects for this system. At the minimum for the correlated interaction, the HF contribution is only -0.39 kcal/mol and is determined by two pairs of large values of opposite signs: the first-order interactions $E_{\text{exch}}^{(10)} + E_{\text{elst}}^{(10)} = 3.88 - 3.62 = +0.26$ kcal/mol and the second-order

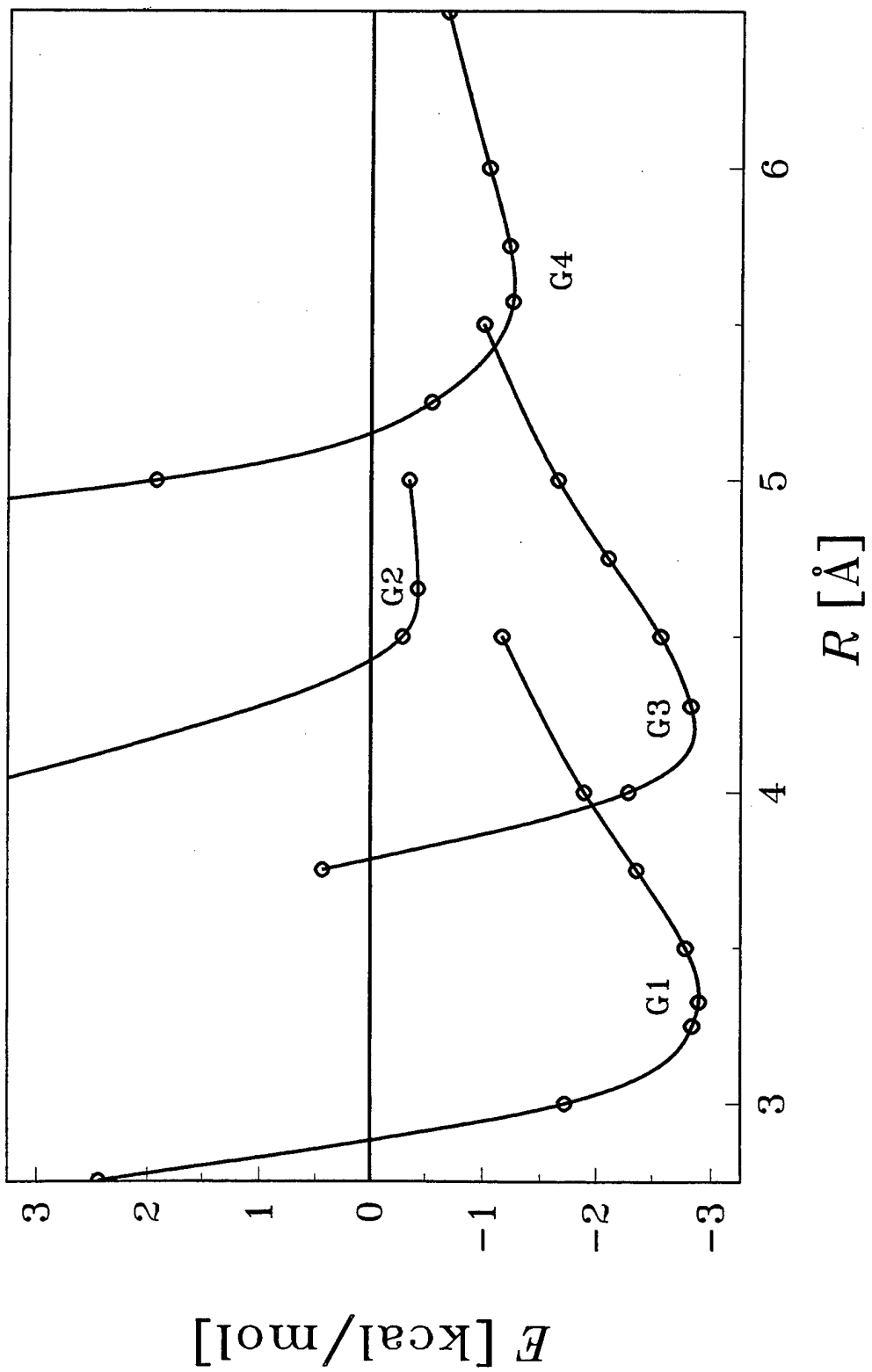


Figure 3. Cuts in R Through the PES for the Four Local Minimum Geometries Detailed in Table 2. The Final Energies Were Computed Using Equation (9) and Include $E_{\text{disp}}^{(20)(+mb)}$. The Solid Line Is a Spline Fit to the Single-Point SAPT Energies for Each Cut and Is Only to Guide the Eye. Energies Are in kcal/mol, and Distances Refer to the Center-of-Mass Separation Between the Two Monomers in \AA .

Table 6. Potential Cuts in R Through the Two Local Minimum Geometries G1 and G2 (All Energies Are in kcal/mol and Distances in Å.)

	G1						G2		
R	2.75	3.00	3.25	3.33	3.50	3.75	4.00	4.50	4.65
$E_{\text{int}}^{\text{HF}}$	9.60	2.80	0.04	-0.39	-0.94	-1.18	-1.14	-0.85	8.94
$E_{\text{elst}}^{(1)}$	-13.00	-7.10	-4.20	-3.64	-2.71	-1.89	-1.40	-0.86	-2.79
$E_{\text{exch}}^{(1)}$	25.50	11.33	5.00	3.88	2.19	0.96	0.42	0.08	13.14
$E_{\text{ind,resp}}^{(20)}$	-13.58	-5.87	-2.58	-2.01	-1.16	-0.54	-0.27	-0.08	-4.33
$E_{\text{exch-ind,resp}}^{(20)}$	11.69	4.94	2.06	1.57	0.85	0.35	0.14	0.02	3.59
δ_{HF}	-1.01	-0.50	-0.23	-0.18	-0.11	-0.05	-0.03	-0.01	-0.67
$\varepsilon_{\text{elst,resp}}^{(1)}(3)$	0.77	0.68	0.57	0.53	0.46	0.37	0.29	0.19	-0.71
$\varepsilon_{\text{exch}}^{(1)}(2)$	1.23	0.64	0.31	0.25	0.15	0.07	0.03	0.01	1.26
$'E_{\text{ind}}^{(22)}$	-0.09	0.03	0.05	0.05	0.04	0.03	0.02	0.01	-0.37
$'E_{\text{exch-ind}}^{(22)}$	0.07	-0.03	-0.04	-0.04	-0.03	-0.02	-0.01	0.00	0.31
$E_{\text{disp}}^{(20)}$	-9.09	-5.62	-3.53	-3.07	-2.26	-1.47	-0.98	-0.46	-5.11
$E_{\text{disp}}^{(21)}$	2.44	1.46	0.90	0.78	0.57	0.38	0.25	0.12	0.70
$E_{\text{disp}}^{(22)}$	-2.36	-1.47	-0.93	-0.81	-0.60	-0.39	-0.27	-0.13	-1.00
$\varepsilon_{\text{disp}}^{(2)}(2)$	0.09	0.00	-0.03	-0.03	-0.03	-0.02	-0.01	0.00	-0.30
$E_{\text{disp}}^{(2)}$	-9.00	-5.62	-3.55	-3.09	-2.28	-1.49	-0.99	-0.47	-5.42

Table 6. Potential Cuts in R Through the Two Local Minimum Geometries G1 and G2 (All Energies Are in kcal/mol and Distances in Å.) (continued)

R	G1					G2						
	2.75	3.00	3.25	3.33	3.50	3.75	4.00	4.50	4.00	4.50	4.65	5.00
$E_{\text{exch-disp}}^{(20)}$	1.70	0.84	0.41	0.32	0.19	0.09	0.04	0.01	0.72	0.14	0.08	0.02
E_{int} ^{corr}	-5.32	-3.45	-2.26	-1.98	-1.47	-0.96	-0.62	-0.26	-4.21	-1.91	-1.52	-0.91
E_{int}	4.28	-0.66	-2.22	-2.37	-2.41	-2.14	-1.76	-1.11	4.73	0.01	-0.22	-0.26
$E_{\text{disp}}^{(20)(+\text{mb})}$	-10.92	-6.69	-4.14	-3.60	-2.62	-1.69	-1.12	-0.52	-6.11	-2.23	-1.67	-0.90
$E_{\text{int}}^{(+\text{mb})}$	2.45	-1.72	-2.84	-2.90	-2.78	-2.36	-1.89	-1.16	3.73	-0.29	-0.43	-0.35

Table 7. Potential Cuts in R Through the Local Minimum Geometry G3 (All Energies Are in kcal/mol and Distances in Å.)

R	3.75	4.00	4.28	4.50	4.75	5.00	5.50
$E_{\text{int}}^{\text{HF}}$	5.03	0.54	-1.13	-1.44	-1.39	-1.20	-0.82
$E_{\text{elst}}^{(10)}$	-11.29	-6.16	-3.52	-2.43	-1.72	-1.28	-0.79
$E_{\text{exch}}^{(10)}$	18.84	7.87	2.96	1.32	0.53	0.21	0.03
$E_{\text{ind, resp}}^{(20)}$	-9.30	-3.71	-1.42	-0.69	-0.33	-0.18	-0.07
$E_{\text{exch-ind, resp}}^{(20)}$	7.48	2.84	0.96	0.40	0.14	0.05	0.01
δ^{HF}	-0.70	-0.29	-0.10	-0.04	-0.02	-0.01	0.00
$\varepsilon_{\text{elst, resp}}^{(1)}(3)$	-0.30	0.01	0.15	0.18	0.17	0.16	0.11
$\varepsilon_{\text{exch}}^{(1)}(2)$	2.13	1.14	0.53	0.28	0.13	0.06	0.01
$tE_{\text{ind}}^{(22)}$	-1.17	-0.51	-0.19	-0.08	-0.03	-0.01	0.00
$tE_{\text{exch-ind}}^{(22)}$	0.94	0.39	0.13	0.05	0.01	0.00	0.00
$E_{\text{disp}}^{(20)}$	-5.91	-3.55	-2.06	-1.36	-0.87	-0.58	-0.28
$E_{\text{disp}}^{(21)}$	1.51	0.87	0.50	0.33	0.22	0.15	0.07
$E_{\text{disp}}^{(22)}$	-1.72	-1.03	-0.61	-0.40	-0.26	-0.17	-0.08
$\varepsilon_{\text{disp}}^{(2)}(2)$	-0.21	-0.16	-0.11	-0.07	-0.04	-0.02	-0.01
$E_{\text{disp}}^{(2)}(2)$	-6.12	-3.71	-2.17	-1.43	-0.92	-0.60	-0.28
$E_{\text{exch-disp}}^{(20)}$	1.15	0.54	0.23	0.11	0.04	0.02	0.00
$E_{\text{int}}^{\text{corr}}$	-3.37	-2.14	-1.33	-0.90	-0.58	-0.38	-0.15
E_{int}	1.66	-1.60	-2.45	-2.34	-1.97	-1.58	-0.97
$E_{\text{disp}}^{(20)(+\text{mb})}$	-7.13	-4.24	-2.43	-1.58	-1.00	-0.66	-0.30
$E_{\text{int}}^{(+\text{mb})}$	0.44	-2.29	-2.82	-2.57	-2.10	-1.66	-1.00

Table 8. Potential Cuts in R Through the Local Minimum Geometry G4 (All Energies Are in kcal/mol and Distances in Å.)

R	4.75	5.00	5.25	5.57	5.75	6.00	6.50
$E_{\text{int}}^{\text{HF}}$	14.29	5.11	1.43	-0.15	-0.43	-0.54	-0.48
$E_{\text{elst}}^{(10)}$	-8.55	-3.89	-2.00	-1.08	-0.85	-0.66	-0.46
$E_{\text{exch}}^{(10)}$	24.74	9.84	3.82	1.09	0.54	0.20	0.03
$E_{\text{ind, resp}}^{(20)}$	-6.43	-2.22	-0.81	-0.26	-0.15	-0.08	-0.04
$E_{\text{exch-ind, resp}}^{(20)}$	5.67	1.92	0.64	0.15	0.07	0.02	0.00
δ^{HF}	-1.15	-0.53	-0.21	-0.05	-0.02	-0.01	0.00
$\varepsilon_{\text{elst, resp}}^{(1)}(3)$	-0.48	-0.12	0.04	0.11	0.12	0.12	0.09
$\varepsilon_{\text{exch}}^{(1)}(2)$	2.16	1.15	0.56	0.20	0.11	0.05	0.01
$E_{\text{ind}}^{(22)}$	-0.99	-0.38	-0.14	-0.03	-0.01	0.00	0.00
$E_{\text{exch-ind}}^{(22)}$	0.88	0.33	0.11	0.02	0.01	0.00	0.00
$E_{\text{disp}}^{(20)}$	-6.38	-3.74	-2.25	-1.21	-0.88	-0.58	-0.27
$E_{\text{disp}}^{(21)}$	1.19	0.65	0.38	0.21	0.16	0.11	0.05
$E_{\text{disp}}^{(22)}$	-1.30	-0.80	-0.50	-0.29	-0.22	-0.15	-0.08
$\varepsilon_{\text{disp}}^{(2)}(2)$	-0.11	-0.14	-0.12	-0.08	-0.06	-0.04	-0.02
$E_{\text{disp}}^{(2)}(2)$	-6.49	-3.88	-2.37	-1.30	-0.95	-0.62	-0.29
$E_{\text{exch-disp}}^{(20)}$	1.12	0.51	0.22	0.07	0.04	0.62	0.00
$E_{\text{int}}^{\text{corr}}$	-3.80	-2.39	-1.57	-0.92	-0.68	-0.44	-0.19
E_{int}	10.49	2.73	-0.14	-1.07	-1.11	-0.98	-0.66
$E_{\text{disp}}^{(20)(+\text{mb})}$	-7.94	-4.55	-2.66	-1.39	-0.99	-0.64	-0.29
$E_{\text{int}}^{(+\text{mb})}$	8.93	1.92	-0.55	-1.25	-1.22	-1.04	-0.68

$E_{\text{exch-ind,resp}}^{(20)} + E_{\text{ind,resp}}^{(20)} = 1.57 - 2.01 = -0.44 \text{ kcal/mol}$. The resulting two values of opposite signs, plus the residual $\epsilon = -0.18$ [see equation (8)], produce the comparatively small -0.39 kcal/mol contribution by the $E_{\text{int}}^{\text{HF}}$. Therefore, the correlated interaction terms account for most of the -2.90 kcal/mol stabilization energy $E_{\text{int}}^{(+\text{mb})}$ near the minimum. It is worth pointing out that even though the net HF induction energy is only -0.44 kcal/mol , it still represents 15% of the total $E_{\text{int}}^{(+\text{mb})} = -2.90 \text{ kcal/mol}$.

Closer examination of Figure 4a shows that almost all of the stabilizing energy comes from the dispersion energy. The intramonomer electron correlation contributions, $E_{\text{disp}}^{(21)}$ and $E_{\text{disp}}^{(22)}$, essentially cancel one another, making a very small net attractive contribution [the sum is labeled as $\epsilon_{\text{disp}}^{(2)}(2)$]. Table 6 shows that at the G1 conformation, $\epsilon_{\text{disp}}^{(2)}(2)$ contributes only 1% of the total dispersion energy. In general, $\epsilon_{\text{disp}}^{(2)}(2)$ accounts for no more than about 10% of the leading-order component, $E_{\text{disp}}^{(20)(+\text{mb})}$, and for about two-thirds of all of the points computed, this contribution is less than 5%. The primary source of the stabilization of the G1 complex can be pinpointed to the leading-order dispersion term $E_{\text{disp}}^{(20)(+\text{mb})}$.

Moving away from the G1 minimum to larger intermolecular distances, the stabilization energy at $R = 3.75 \text{ \AA}$ (see Figure 4a) is composed of nearly equal contributions from the dispersion term and the HF energy. The delicate balance between the first- ($E_{\text{elst}}^{(10)}$ and $E_{\text{exch}}^{(10)}$) and second- ($E_{\text{ind,resp}}^{(20)}$ and $E_{\text{exch-ind,resp}}^{(20)}$) order interactions contributing to $E_{\text{int}}^{\text{HF}}$ is shown in Figure 4b. Table 6 shows that the repulsive first-order exchange energy is a major contributor to $E_{\text{int}}^{\text{HF}}$ over most of the cut through G1 and counters the large stabilizing interaction arising from the electrostatic term $E_{\text{elst}}^{(10)}$. This gives a

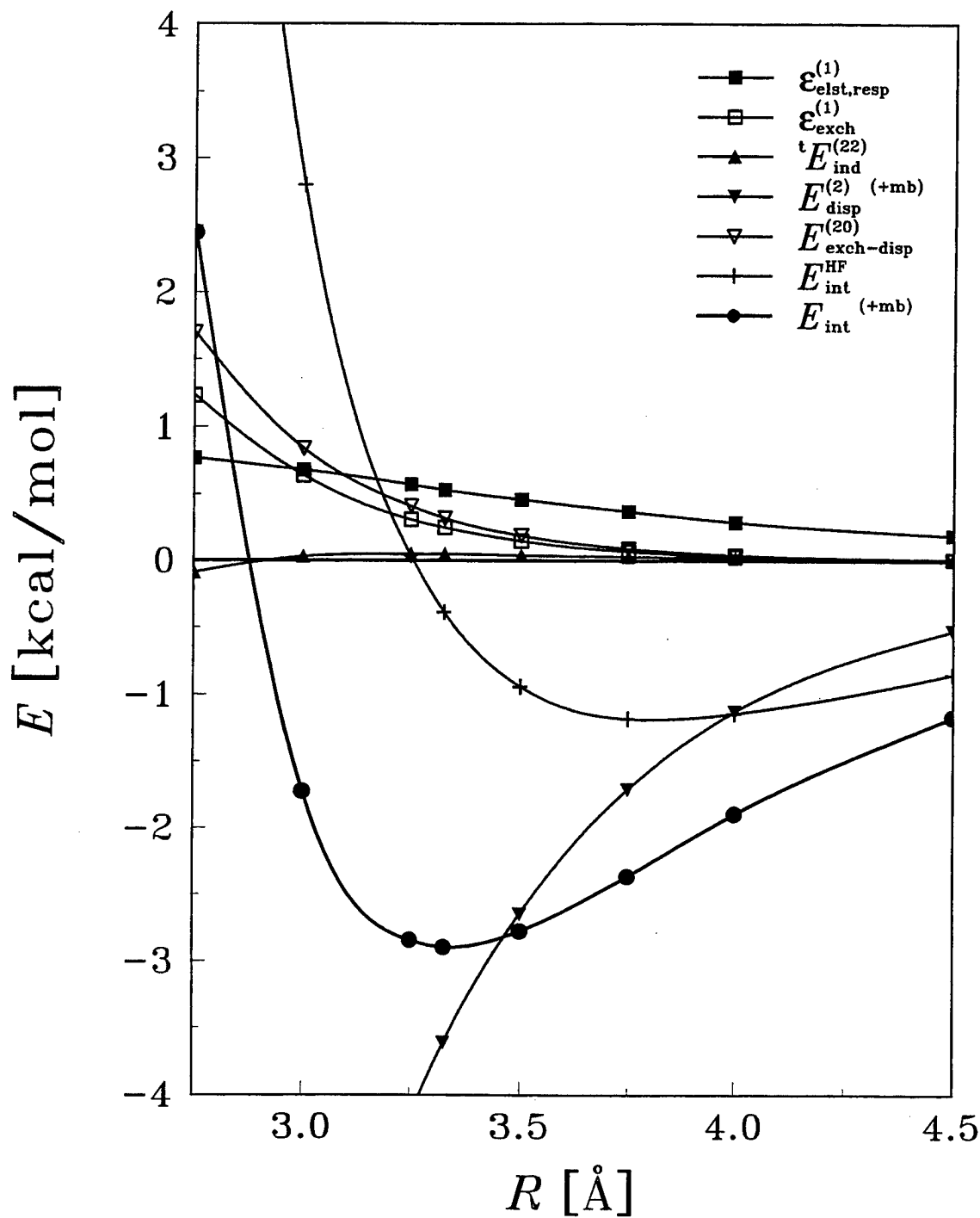


Figure 4a. SAPT Components Used in Equation (9) for a Range of R Values at and Around the Local Minimum Geometry G1. The Estimated Component $tE_{\text{exch-ind}}^{(22)}$ Is Not Included in the Figure. The Numerical Results for This Cut Are Displayed in Table 6. The Energies and Distances Are Given in Units of kcal/mol and Å, Respectively.

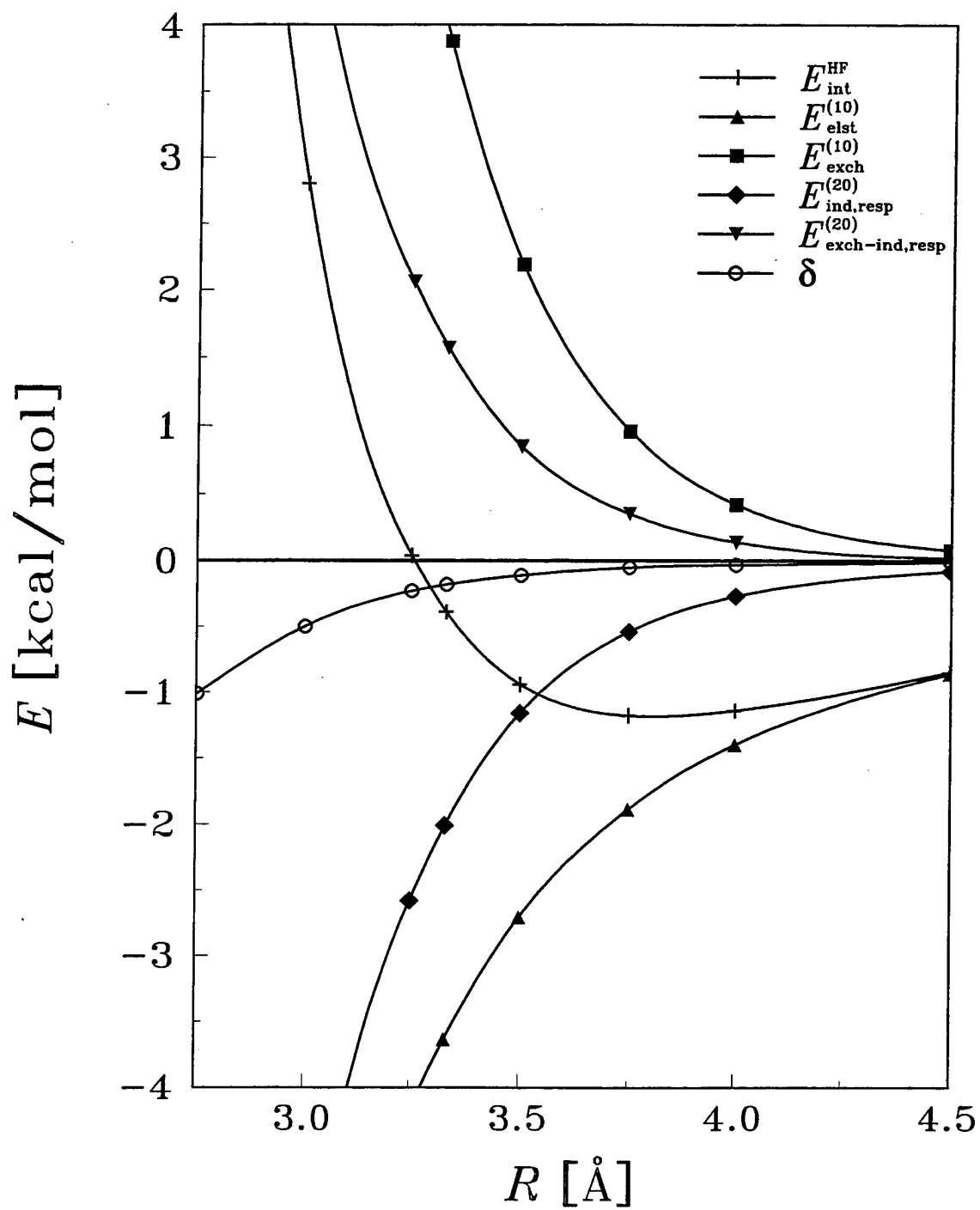


Figure 4b. $E_{\text{int}}^{\text{HF}}$ and the SAPT Components Included in Equation (8) at and Around Geometry G1 as a Function of R .

net HF first-order contribution of $E_{\text{elst}}^{(10)} + E_{\text{exch}}^{(10)} = -0.93$ kcal/mole, or 39% of the total interaction energy at $R = 3.75 \text{ \AA}$. While this is also a general trend, the G2 geometry is a notable exception. Table 6 shows the G2 HF electrostatic term $E_{\text{elst}}^{(10)}$ to be repulsive, with a value of +0.33 kcal/mol near the minimum at $R = 4.65 \text{ \AA}$. Returning to the G1 geometry, the induction energy ($E_{\text{ind,resp}}^{(20)}$) accounts for 22% of the stabilization interactions at $R = 3.75 \text{ \AA}$, which gives a net HF second-order contribution of $E_{\text{ind,resp}}^{(20)} + E_{\text{exch-ind,resp}}^{(20)} = -0.19$, or 8% of the total interaction energy.

A summary of the individual components split according to equation (9) for all four geometries, G1, G2, G3, and G4, are shown in histogram format in Figure 5a. A quick inspection shows that the $E_{\text{disp}}^{(2)(+mb)}$ energy is the largest component in absolute value for each of these configurations. Also, it is clear that $E_{\text{int}}^{\text{HF}}$ plays an important role in determining the total interaction energy at two of the four minimum geometries, specifically G2 and G3. For all configurations except G2, the $E_{\text{int}}^{\text{HF}}$ energy stabilizes the complex.

A histogram for the components of $E_{\text{int}}^{\text{HF}}$ for these four geometries is given in Figure 5b. The repulsive contribution of $E_{\text{int}}^{\text{HF}}$ for G2 differs from the other three minima by having a positive electrostatic interaction energy (i.e., $E_{\text{elst}}^{(10)} = +0.33$ kcal/mol). In the other three minimum conformations, $E_{\text{elst}}^{(10)}$ is negative and nearly cancels the positive $E_{\text{exch}}^{(10)}$ term. Hence, as seen in Table 6, the combination of the positive electrostatic term and a large (positive) $E_{\text{exch}}^{(10)}$ account for the very weak bond at this geometry. Finally, for configurations G1 and G4, Figure 5b illustrates the cancellation within the first-order and second-order HF terms, leaving $E_{\text{disp}}^{(2)(+mb)}$ as the dominant contribution to the total interaction energy.

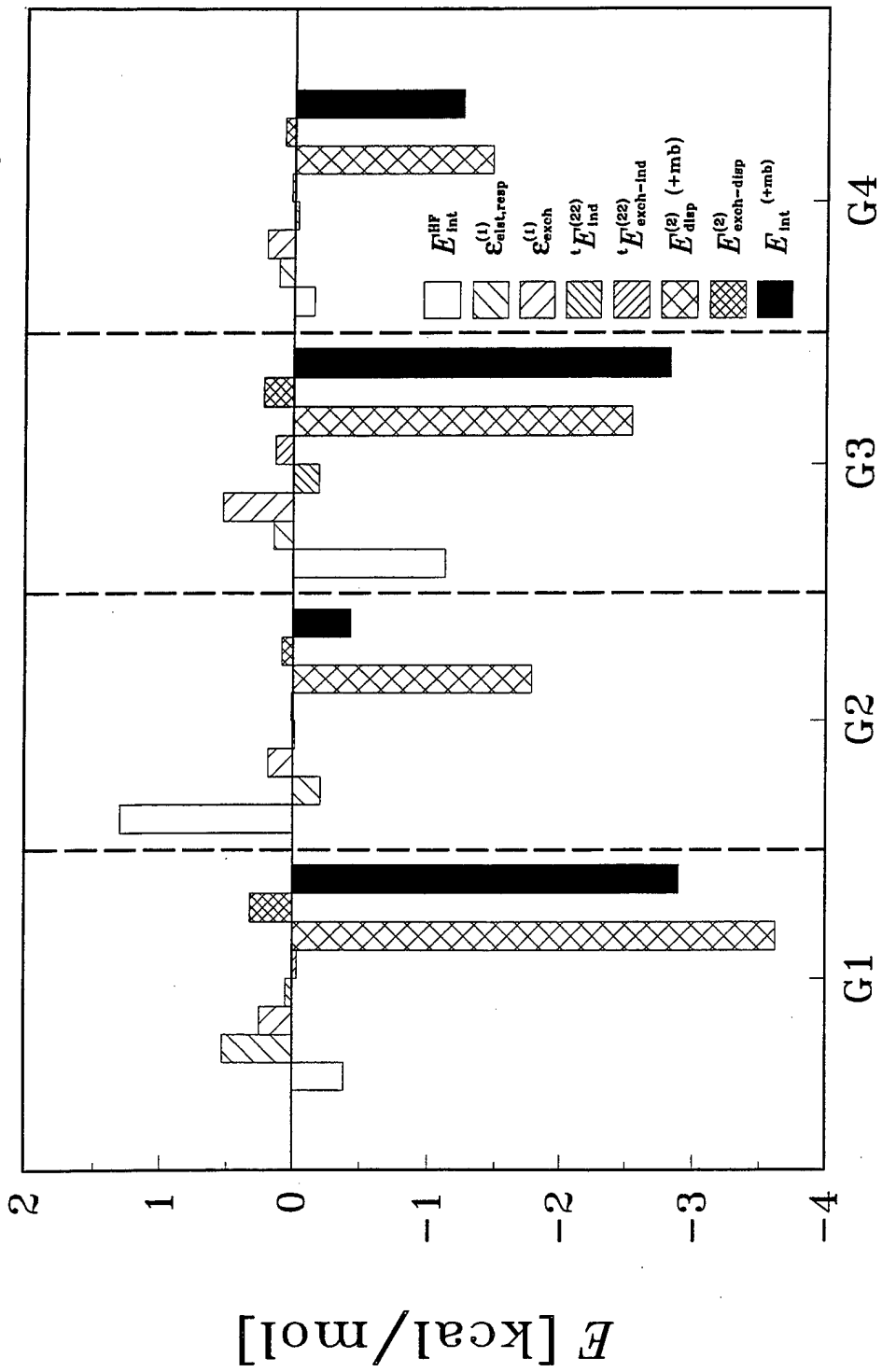
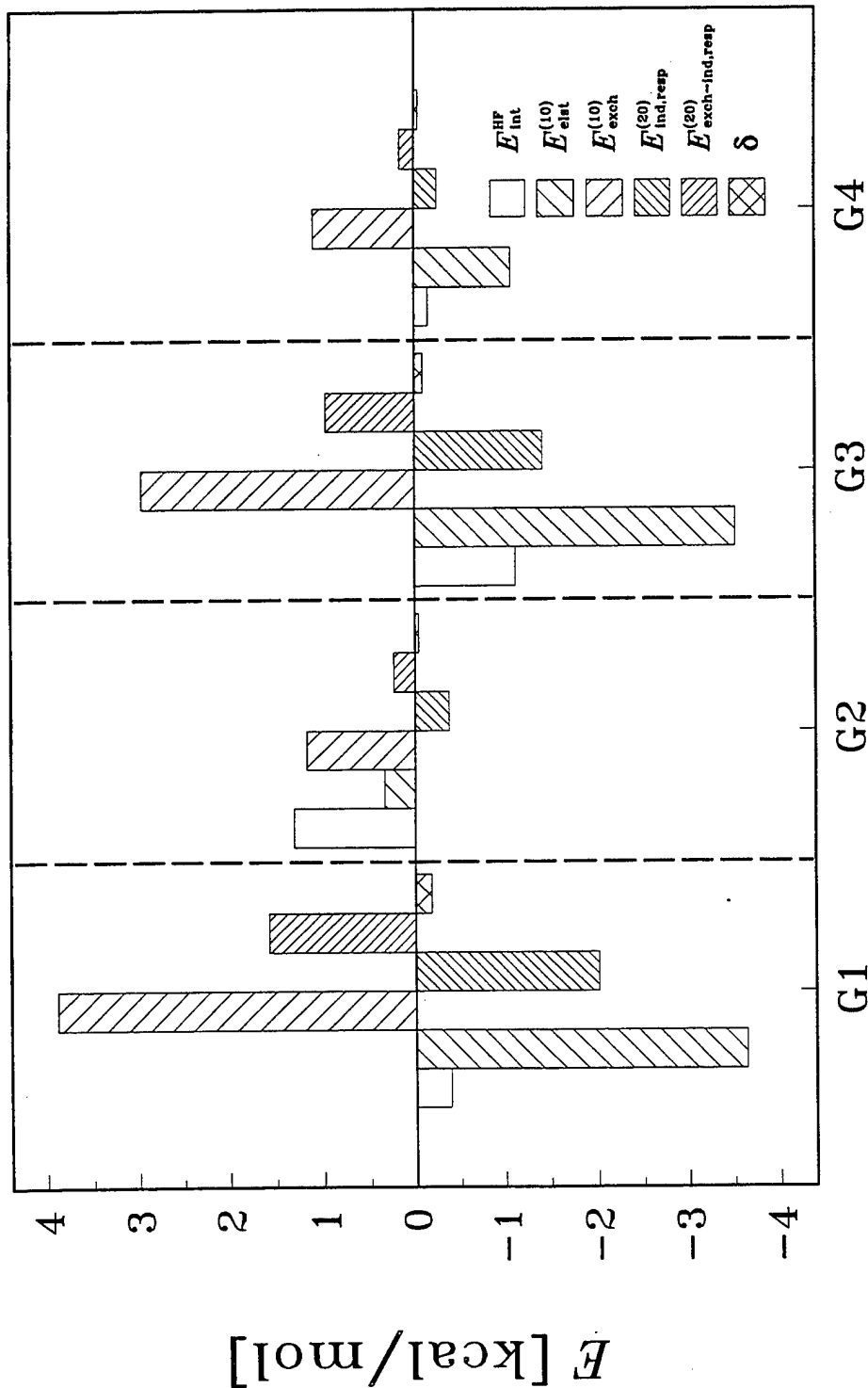


Figure 5a. The Interaction Energy and Individual Components Indicated in Equation (9) Are Shown in Histogram Format to Illustrate the Relative Importance of the Various Energy Contributions at the G1, G2, G3, and G4 Minima.

Figure 5b. A Histogram Is Shown Containing $E_{\text{int}}^{\text{HF}}$ and the SAPT Components Included in Equation (8) at the G1, G2, G3, and G4 Minima.



Tables 9 and 10 provide the interaction energies on the PES around geometry G1 as a function of β_1 for three values of R . Figure 6 displays the β_1 dependence of the total interaction energy at $R = 4.0$ and 4.75 \AA . Figure 6 clearly shows the asymmetry in β_1 for the $R = 4.0 \text{ \AA}$ cut due to the absence of a σ_h symmetry plane in CH_3CN . At $R = 4.75 \text{ \AA}$, the PES flattens out and is attractive everywhere as a function of the single variable β_1 , albeit weakly bound. These plots predict a favorable angle β_1 of approach in the range $80^\circ \leq \beta_1 \leq 150^\circ$.

Analyses of the terms defining the total $E_{\text{int}}^{(+\text{mb})}$ are shown in Figures 7 and 8 for $R = 4.0$ and 4.75 \AA , respectively. Figure 7a plots the components of $E_{\text{int}}^{(+\text{mb})}$ [according to equation (9)] as a function of β_1 at $R = 4.0 \text{ \AA}$. Again, $E_{\text{int}}^{(+\text{mb})}$ is determined primarily by two terms, $E_{\text{int}}^{\text{HF}}$ and $E_{\text{disp}}^{(2)(+\text{mb})}$. The remaining terms from $E_{\text{int}}^{\text{corr}}$ are small in absolute magnitude and essentially cancel one another. Table 9 indicates that the leading-order dispersion term, $E_{\text{disp}}^{(20)(+\text{mb})}$, accounts for most of the net contribution to the total dispersion interaction. The $E_{\text{disp}}^{(21)}$ and $E_{\text{disp}}^{(22)}$ energies are individually 28% or less of the $E_{\text{disp}}^{(20)}$ energy, but are nearly equal in magnitude and opposite in sign, effectively canceling one another. This cancellation of dispersion components was noted earlier in the analysis of $E_{\text{int}}^{(+\text{mb})}$ as a function of R .

The separation of $E_{\text{int}}^{\text{HF}}$ into the components indicated in equation (8) is shown in Figure 7b. The second-order terms, $E_{\text{exch-ind,resp}}^{(20)}$ and $E_{\text{ind,resp}}^{(20)}$, practically cancel over the entire range of β_1 . Thus, the general dependence of $E_{\text{int}}^{\text{HF}}$ on β_1 can be assigned to the two first-order terms $E_{\text{exch}}^{(10)}$ and $E_{\text{elst}}^{(10)}$. As β_1 goes to 180° , the atoms of the CO_2 molecule come into closer proximity with atoms on CH_3CN . At $\beta_1 = 180^\circ$, an oxygen resides only 1.95 \AA away from the nitrogen. In this arrangement, one would expect a repulsive intermolecular penetration of the electron clouds by the two monomers (i.e., a “steric” interaction, and indeed the exchange [repulsion] interaction dominates near 180°).

Table 9. Potential Cuts in β_1 at Geometry G1 for Two Different R Values (All Energies Are in kcal/mol and Distances in Å. Only Two Angles Are Shown for the R Value Taken From Geometry G1, Since Each of the Others Is Too High on the Exponential Wall.)

R	G1			4.0			
	β_1	90°	135°	45°	90°	108°	135°
$E_{\text{int}}^{\text{HF}}$	1.58	4.16	11.04	-0.8	-1.14	-1.01	9.59
$E_{\text{elst}}^{(10)}$	-3.5	-8.45	-6.13	-1.14	-1.40	-2.41	-8.92
$E_{\text{exch}}^{(10)}$	5.82	14.31	18.46	0.5	0.42	1.74	20.09
$E_{\text{ind, resp}}^{(20)}$	-1.91	-7.76	-5.64	-0.23	-0.27	-0.9	-8.22
$E_{\text{exch-ind, resp}}^{(20)}$	1.50	6.58	5.16	0.1	0.14	0.64	7.24
δ^{HF}	-0.32	-0.53	-0.81	-0.03	-0.03	-0.08	-0.59
$\varepsilon_{\text{elst, resp}}^{(1)}(3)$	0.24	0.43	-0.32	0.21	0.29	0.29	-0.56
$\varepsilon_{\text{exch}}^{(1)}(2)$	0.58	0.68	1.13	0.08	0.03	0.13	1.52
$E_{\text{ind}}^{(22)}$	-0.14	-0.06	-0.64	0.00	0.02	0.01	-1.26
$E_{\text{exch-ind}}^{(22)}$	0.11	0.05	0.58	0.00	-0.01	-0.01	1.11
$E_{\text{disp}}^{(20)}$	-3.57	-5.55	-5.13	-1.09	-0.98	-1.64	-5.57
$E_{\text{disp}}^{(21)}$	0.80	1.48	0.78	0.25	0.25	0.41	1.46
$E_{\text{disp}}^{(22)}$	-0.88	-1.43	-0.96	-0.29	-0.27	-0.42	-1.55
$\varepsilon_{\text{disp}}^{(2)}(2)$	-0.08	-0.05	-0.17	-0.03	-0.01	-0.01	-0.1
$E_{\text{disp}}^{(2)}(2)$	-3.65	-5.5	-5.3	-1.12	-0.99	-1.65	-5.66
$E_{\text{exch-disp}}^{(20)}$	0.40	1.01	0.95	0.04	0.04	0.15	1.22
$E_{\text{corr int}}$	-2.46	-3.38	-3.61	-0.79	-0.62	-1.08	-3.62
E_{int}	-0.88	0.78	7.43	-1.59	-1.76	-2.09	5.97
$E_{\text{disp}}^{(20)(+\text{mb})}$	-4.11	-6.74	-6.04	-1.21	-1.12	-1.95	-6.75
$E_{\text{int}}^{(+\text{mb})}$	-1.41	-0.41	6.52	-1.71	-1.89	-2.4	4.79

Table 10. Potential Cuts in β_1 at Geometry G1 for $R = 4.75 \text{ \AA}$ (All Energies Are in kcal/mol.)

β_1	45°	90°	135°	180°
$E_{\text{int}}^{\text{HF}}$	0.55	-0.83	-0.93	0.11
$E_{\text{elst}}^{(10)}$	-0.56	-0.83	-1.00	-1.15
$E_{\text{exch}}^{(10)}$	1.28	0.06	0.15	1.56
$E_{\text{ind,resp}}^{(20)}$	-0.34	-0.07	-0.12	-0.60
$E_{\text{exch-ind,resp}}^{(20)}$	0.24	0.02	0.04	0.38
δ^{HF}	-0.07	0.00	-0.01	-0.07
$\varepsilon_{\text{elst,resp}}^{(1)}(3)$	0.00	0.17	0.16	-0.02
$\varepsilon_{\text{exch}}^{(1)}(2)$	0.16	0.00	0.02	0.27
$E_{\text{ind}}^{(22)}$	-0.04	0.01	0.01	-0.11
$E_{\text{exch-ind}}^{(22)}$	0.03	0.00	-0.00	0.07
$E_{\text{disp}}^{(20)}$	-1.17	-0.37	-0.50	-1.29
$E_{\text{disp}}^{(21)}$	0.16	0.10	0.13	0.32
$E_{\text{disp}}^{(22)}$	-0.25	-0.10	-0.13	-0.39
$\varepsilon_{\text{disp}}^{(2)}(2)$	-0.09	-0.00	-0.00	-0.07
$E_{\text{disp}}^{(2)}(2)$	-1.26	-0.37	-0.50	-1.35
$E_{\text{exch-disp}}^{(20)}$	0.09	0.01	0.01	0.13
$E_{\text{int}}^{\text{corr}}$	-1.02	-0.19	-0.30	-1.02
E_{int}	-0.47	-1.02	-1.23	-0.91
$E_{\text{disp}}^{(20)(+\text{mb})}$	-1.34	-0.38	-0.57	-1.50
$E_{\text{int}}^{(+\text{mb})}$	-0.64	-1.03	-1.30	-1.12

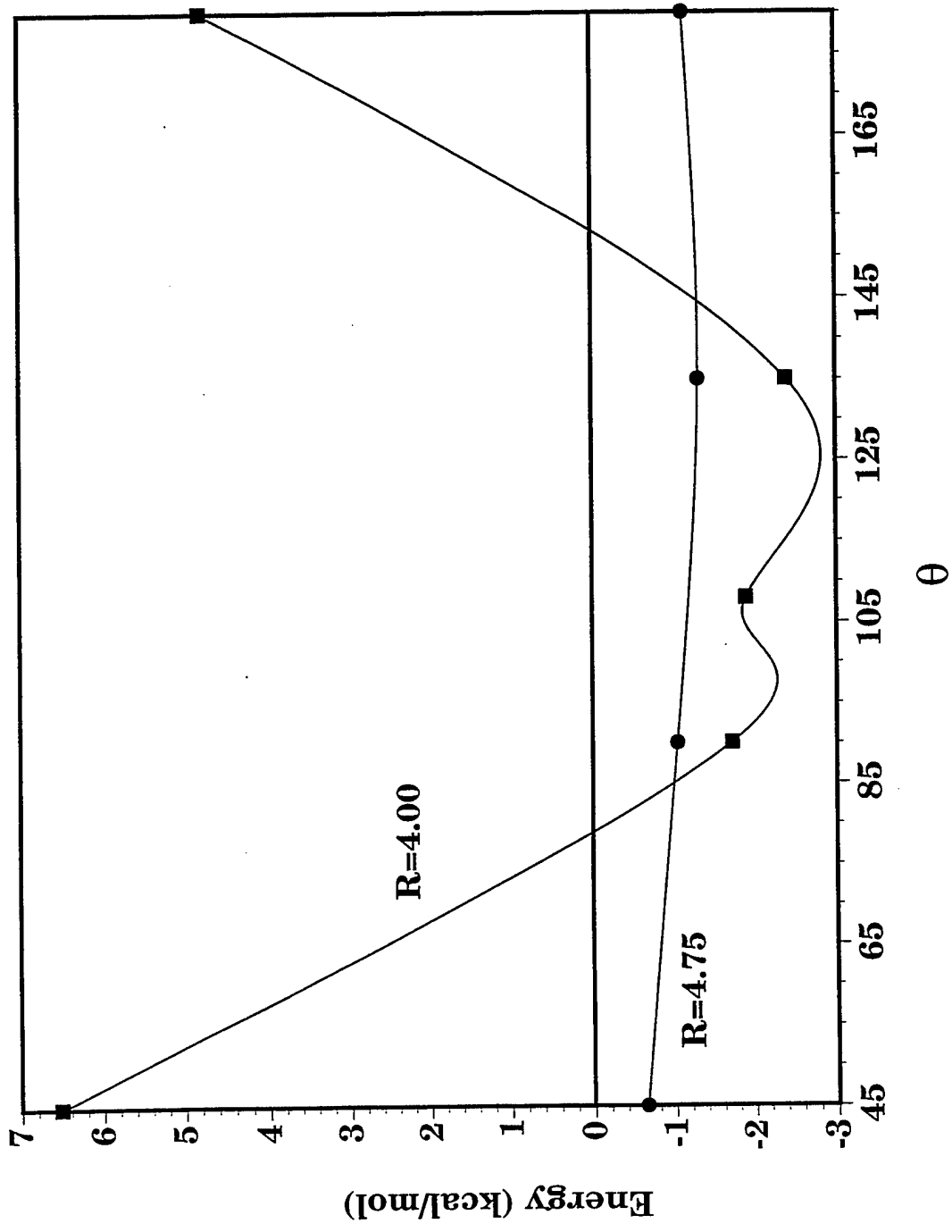


Figure 6. $E_{\text{int}}^{(+\text{mb})}$ as a Function of β_1 Is Shown for $R = 4.0$ and $R = 4.75 \text{ \AA}$, With the Remaining Coordinates Taken From G1. The Solid Line Is a Spline Fit to the Single Point SAPT Energies for These Two Cuts and Is Only to Guide the Eye. (Data Taken From Tables 9 and 10.)

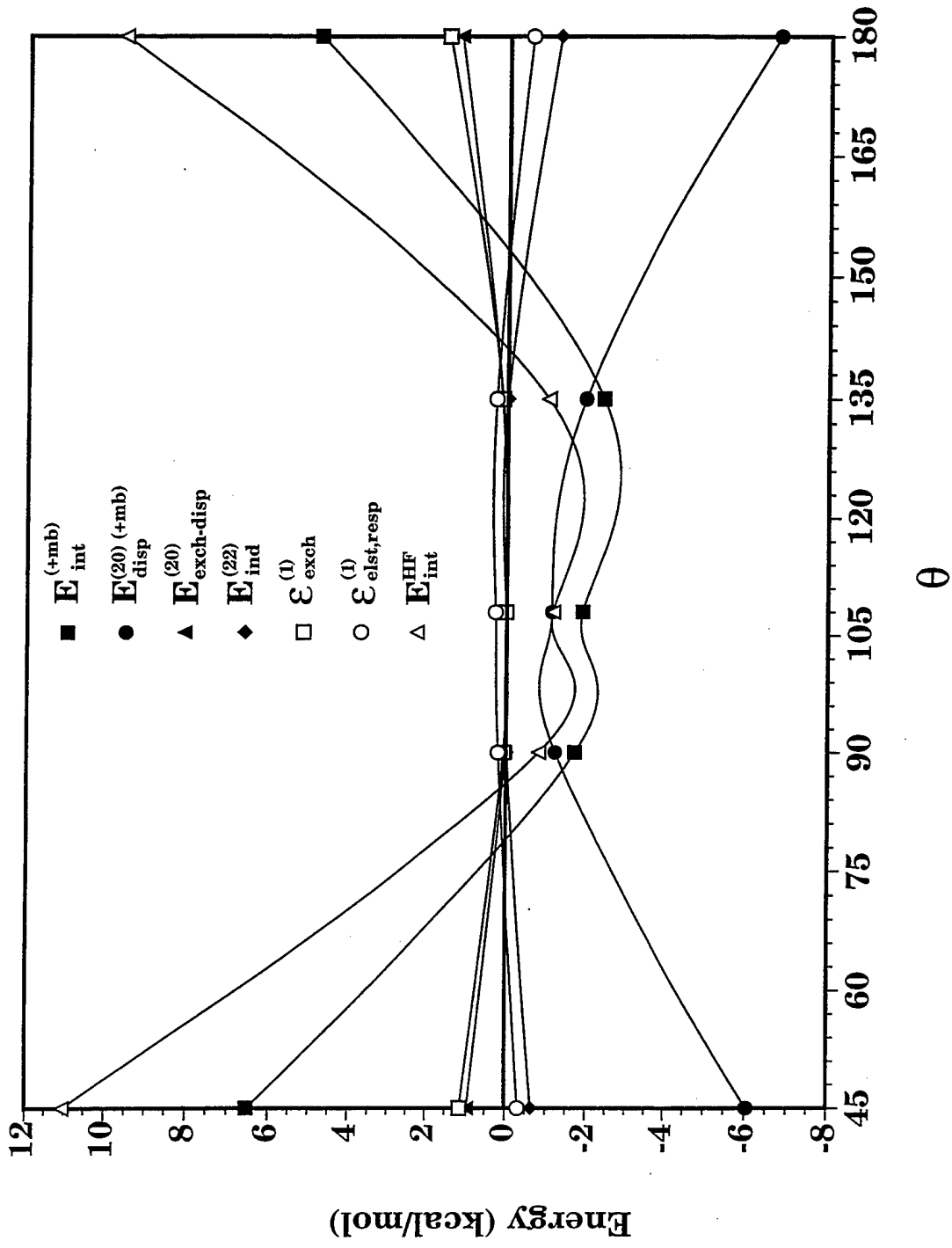


Figure 7a. The Interaction Energy $E_{int}^{(+mb)}$ and Its Components According to Equation (9) Shown as a Function of β_1 for $R = 4.0 \text{ \AA}$.
The Remaining Coordinates Are Those of the G1 Geometry. (Data Taken From Table 9.)

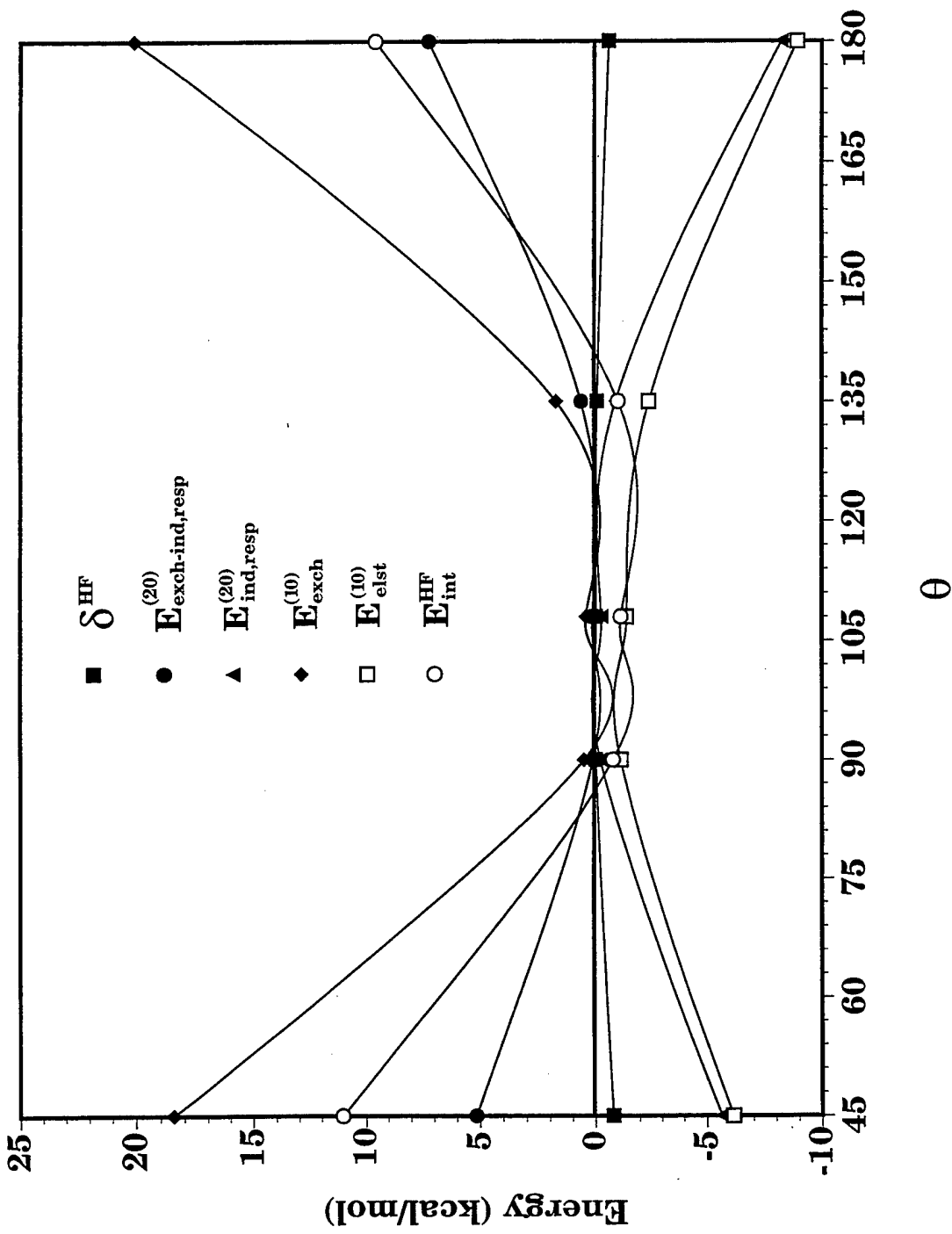


Figure 7b. The HF Interaction Energy $E_{\text{int}}^{\text{HF}}$ and Its Components According to Equation (8) Shown as a Function of β_1 for $R = 4.0 \text{ \AA}$. The Remaining Coordinates Are Those of the G1 Geometry. (Data Taken From Table 9.)

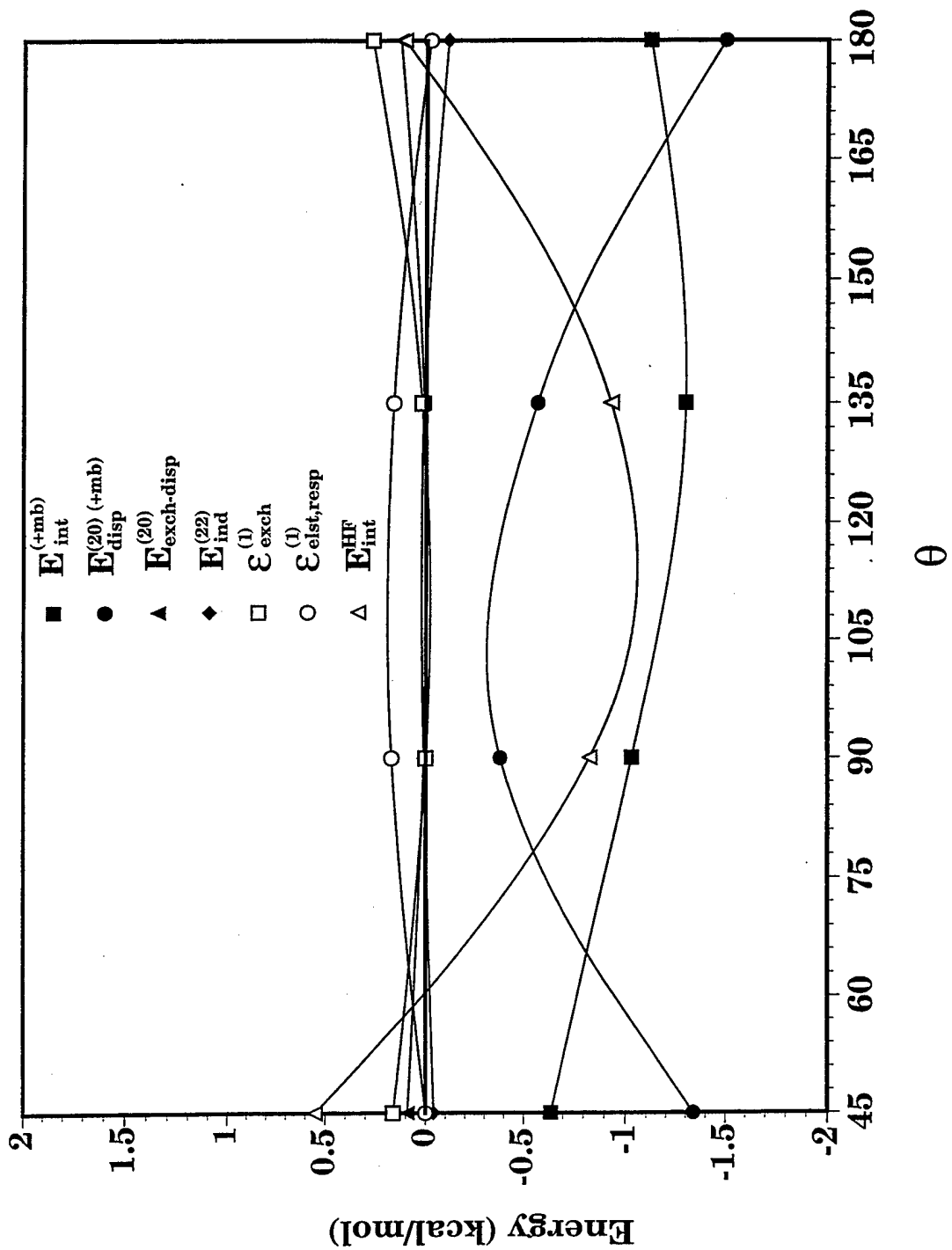


Figure 8a. The Interaction Energy $E_{int}^{(+mb)}$ and Its Components According to Equation (9) Shown as a Function of θ , for $R = 4.75 \text{ \AA}$. The Remaining Coordinates Are Those of the G1 Geometry. (Data Taken From Table 10.)

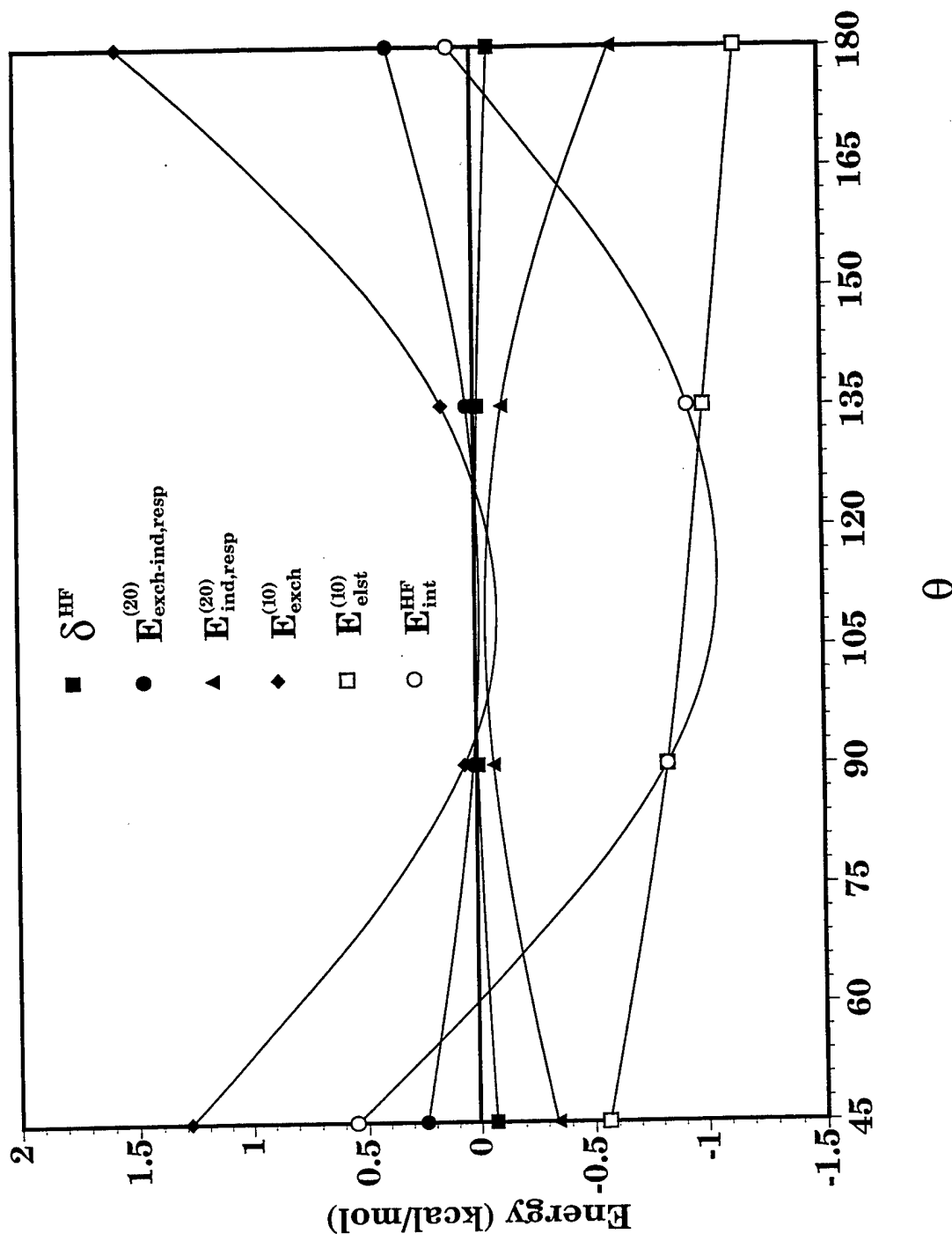


Figure 8b. The HF Interaction Energy $E_{\text{int}}^{\text{HF}}$ and Its Components According to Equation (8) Shown as a Function of β_1 for $R = 4.75 \text{ \AA}$. The Remaining Coordinates Are Those of the G1 Geometry. (Data Taken From Table 10.)

This strong dependence of $E_{\text{exch}}^{(10)}$ on β_1 (indirectly on R) can be seen in Tables 9 and 10 and in Figure 7b as changes in β_1 bring the two molecules closer together. The $E_{\text{exch}}^{(10)}$ term changes from a maximum of +20 kcal/mol at $\beta_1 = 180^\circ$ to 0.4 kcal/mol at 108° (see Table 9).

As the two molecules separate to a distance of $R = 4.75 \text{ \AA}$, Figure 8a shows a similar relationship between the total interaction energy and its components as seen at the shorter $R = 4.0 \text{ \AA}$ distance. As β_1 varies over $45^\circ \leq \beta_1 \leq 180^\circ$, $E_{\text{int}}^{(+\text{mb})}$ is once again seen to be composed primarily of the $E_{\text{int}}^{\text{HF}}$ and $E_{\text{disp}}^{(2)(+\text{mb})}$ contributions, and the dispersion interaction is comprised almost entirely of the leading-order term $E_{\text{disp}}^{(20)(+\text{mb})}$ (see Table 10). $E_{\text{int}}^{\text{HF}}$ is again a balance between the first-order terms $E_{\text{exch}}^{(10)}$ and $E_{\text{elst}}^{(10)}$. From the previous discussion, it is clear that the qualitative, if not quantitative, changes in $E_{\text{int}}^{(+\text{mb})}$ as a function of R and β_1 can be traced primarily to three interaction terms: $E_{\text{elst}}^{(10)}$, $E_{\text{exch}}^{(10)}$, and $E_{\text{disp}}^{(20)(+\text{mb})}$.

5. Conclusions

The $\text{CH}_3\text{CN}-\text{CO}_2$ PES was investigated using SAPT. Approximately 200 geometrical configurations were computed for both selected individual cuts of the PES around the 4 minimum energy geometries and a coarse grid spanning the 5 intermolecular coordinates. A separate computation with a larger basis set, including midbond functions, was also performed at each point for the leading-order dispersion energy. Four representative local minimum geometries were investigated to determine the relative strengths of different physical contributions to the interaction energy. The leading-order dispersion energy, $E_{\text{disp}}^{(20)}$, contributed a large percentage of the binding energy near each of the local minima investigated. Surprisingly, the intramonomer electron correlation corrections to the leading-order dispersion component had very little impact on the final energies due to cancellation between them—even though, individually, they typically had large

absolute magnitudes. The SM HF energy, $E_{\text{int}}^{\text{HF}}$, which includes contributions from the leading-order SAPT components of polarization, exchange, and induction, also had a large though varying impact on the final interaction energy around the local minima investigated. The main contributors to $E_{\text{int}}^{\text{HF}}$ are the first-order exchange and electrostatic terms, where the importance of the electrostatic term is due to the strongly polar nature of the CH₃CN monomer. The most strongly bound geometrical configuration investigated had an interaction energy of -2.90 kcal/mol.

INTENTIONALLY LEFT BLANK.

6. References

1. Allen, M. P., and D. J. Tildesley. *Computer Simulation of Liquids*. Oxford: Clarendon Press, 1987.
2. McHugh, M. A., and V. J. Krukonis. *Supercritical Fluid Extraction: Principles and Practice*. Second edition, Butterworth-Heinemann series in chemical engineering, MA, 1994.
3. Morris, J. B., M. A. Schroeder, R. A. Pesce-Rodriguez, K. L. McNesby, and R. A. Fifer. "Supercritical Fluid Extraction of Nitramine-Based Gun Propellant: A Fluid Survey." ARL-TR-885, U.S. Army Research Laboratory, Aberdeen Proving Ground, MD, 1995.
4. Jeziorski, B., R. Moszynski, and K. Szalewicz. *Chemical Review*. Vol. 94, p. 1887, 1994.
5. Szalewicz, K., and B. Jeziorski. *Molecular Interactions - From van der Waals to Strongly Bound Complexes*. S. Scheiner (editor), New York: Wiley, 1996.
6. Williams, H. L., K. Szalewicz, B. Jeziorski, R. Moszynski, and S. J. Rybak. *Journal of Chemical Physics*. Vol. 98, p. 1279, 1993.
7. Moszynski, R., P. E. S. Wormer, B. Jeziorski, and A. van der Avoird. *Journal of Chemical Physics*. Vol. 101, p. 2811, 1994.
8. Moszynski, R., T. Korona, P. E. S. Wormer, and A. van der Avoird. *Journal of Chemical Physics*. Vol. 103, p. 321, 1995.
9. Lotrich, V. F., H. L. Williams, K. Szalewicz, B. Jeziorski, R. Moszynski, P. E. S. Wormer, and A. van der Avoird. *Journal of Chemical Physics*. Vol. 103, p. 6076, 1995.
10. Moszynski, R., P. E. S. Wormer, and A. van der Avoird. *Journal of Chemical Physics*. Vol. 102, p. 8385, 1995.
11. Jankowski, P., and K. Szalewicz. *Journal of Chemical Physics*. To be published.
12. Mas, E., K. Szalewicz, R. Bukowski, and B. Jeziorski. *Journal of Chemical Physics*. Vol. 107, p. 4207, 1997.
13. Williams, H. L., K. Szalewicz, R. Moszynski, and B. Jeziorski. *Journal of Chemical Physics*. Vol. 103, p. 4586, 1995.
14. Moszynski, R., B. Jeziorski, S. Rybak, K. Szalewicz, and H. L. Williams. *Journal of Chemical Physics*. Vol. 100, p. 5080, 1994.

15. Moszynski, R. M., B. Jeziorski, and K. Szalewicz. *Journal of Chemical Physics*. Vol. 100, p. 1312, 1994.
16. Rybak, S., B. Jeziorski, and K. Szalewicz. *Journal of Chemical Physics*. Vol. 95, p. 6576, 1991.
17. Moszynski, R., B. Jeziorski, and K. Szalewicz. *International Journal of Quantum Chemistry*. Vol. 45, p. 409, 1993.
18. Moszynski, R., B. Jeziorski, A. Ratkiewicz, and S. Rybak. *Journal of Chemical Physics*. Vol. 99, p. 8856, 1993.
19. Moszynski, R., S. M. Cybulski, and G. Chalasinski. *Journal of Chemical Physics*. Vol. 100, p. 4998, 1994.
20. Williams, H. L. "Extensions and Applications of Symmetry-Adapted Perturbation Theory." Ph.D. dissertation, University of Delaware, Newark, DE, 1995.
21. Williams, H. L., T. Korona, R. Bukowski, B. Jeziorski, and K. Szalewicz. *Chemical Physics Letters*. Vol. 262, p. 431, 1996.
22. Korona, T., H. L. Williams, R. Bukowski, B. Jeziorski, and K. Szalewicz. *Journal of Chemical Physics*. Vol. 106, p. 5109, 1997.
23. Jeziorski, M., B. Jeziorski, and J. Cizek. *International Journal of Quantum Chemistry*. Vol. 32, p. 149, 1996.
24. Moszynski, R., T. G. A. Heijmen, and B. Jeziorski. *Molecular Physics*. Vol. 88, p. 741, 1996.
25. Boys, S. F., and R. Bernardi. *Molecular Physics*. Vol. 19, p. 553, 1970.
26. Van Duijneveldt, F. B., J. G. C. M. Duijneveldt-van de Rijdt, and J. H. van Lenthe. *Chemical Review*. Vol. 94, p. 1873, 1994.
27. Dunning, Jr., T. H. *Journal of Chemical Physics*. Vol. 90, p. 1007, 1989.
28. Kendall, R. A., T. H. Dunning, Jr., and R. J. Harrison. *Journal of Chemical Physics*. Vol. 96, p. 6796, 1992.
29. Woon, D. E., and T. H. Dunning, Jr. *Journal of Chemical Physics*. Vol. 98, p. 1358, 1993.
30. Pople, J. A., M. Head-Gordon, and K. Raghavachari. *Journal of Chemical Physics*. Vol. 87, p. 5968, 1987.
31. Salter, E. A., G. Trucks, and R. J. Bartlett. *Journal of Chemical Physics*. Vol. 90, p. 1752, 1989.

32. Foresma, J. B., M. Head-Gordon, J. A. Pople, and M. J. Frisch. *Journal of Physical Chemistry*. Vol. 135, 1996.
33. Sadlej, J., M. M. Szczesniak, and G. Chalasinski. *Journal of Chemical Physics*. Vol. 99, p. 5211, 1993.
34. Frisch, M. J., G. W. Trucks, H. B. Schlegel, P. M. W. Gill, B. G. Johnson, M. A. Robb, J. R. Cheeseman, T. Keith, G. A. Petersson, J. A. Montgomery, K. Raghavachari, M. A. Al-Laham, V. G. Zakrzewski, J. V. Ortiz, J. B. Foresman, J. Cioslowski, B. B. Stefanov, A. Nanayakkara, M. Challacombe, C. Y. Peng, P. Y. Ayala, W. Chen, M. W. Wong, J. L. Andres, E. S. Replogle, R. Gomperts, R. L. Martin, D. J. Fox, J. S. Binkley, D. J. Defrees, J. Baker, J. P. Stewart, M. Head-Gordon, C. Gonzalez, and J. A. Pople. *Gaussian 94*. Revision D.2., Gaussian, Inc., Pittsburgh, PA, 1995.
35. Saunders, V. R., and M. F. Guest. *ATMOL Program Package*. SERC Daresbury Laboratory, Daresbury, Great Britain.
36. Jeziorski, B., R. Moszynski, A. Ratkiewicz, S. Rybak, K. Szalewicz, and H. L. Williams. *Methods and Techniques in Computational Chemistry: METECC94, Vol. B Medium-Size Systems*. STEF, E. Clementi (editor), Cagliari, Italy, 1993, p. 79. The SAPT suite of codes is also available directly from the authors. For more information, contact Krzysztof Szalewicz, Department of Physics and Astronomy, University of Delaware, Newark, DE 19716 or by e-mail at szalewic@udel.edu.
37. Brink, D. M., and G. R. Satchler. *Angular Momentum*. Clarendon, Oxford, 1975.
38. Williams, H. L., E. M. Mas, K. Szalewicz, and B. Jeziorski. *Journal of Chemical Physics*. Vol. 103, p. 7374, 1995.
39. Raffenetti, R. *Journal of Chemical Physics*. Vol. 58, p. 4452, 1973.
40. Frisch, M. J., J. A. Pople, and J. S. Binkley. *Journal of Chemical Physics*. Vol. 80, p. 3265, 1984.
41. Weast, R. C. (editor). *CRC Handbook of Chemistry and Physics*. Boca Raton, FL: CRC Press, Inc., 64th edition, 1984.
42. Graham, C., J. Pierrus, and R. E. Raab. *Molecular Physics*. Vol. 67, p. 939, 1989.
43. Budenholzer, F. E., E. A. Gislason, A. D. Jorgensen, and J. G. Sachs. *Chemical Physics Letters*. Vol. 47, p. 429, 1977.
44. Ho, W., G. Birnbaum, and A. Rosenberg. *Journal of Chemical Physics*. Vol. 55, p. 1028, 1971.

44. Ho, W., G. Birnbaum, and A. Rosenberg. *Journal of Chemical Physics*. Vol. 55, p. 1028, 1971.
45. Bose, T. K., and R. H. Cole. *Journal of Chemical Physics*. Vol. 52, p. 140, 1989.

Appendix:

**Supporting Information for Investigation of the
CH₃CN-CO₂ Potential Energy Surface (PES) Using
Symmetry-Adapted Perturbation Theory (SAPT)**

INTENTIONALLY LEFT BLANK.

Table A-1. The Supplementary Tables Complement Tables 6–10 and Provide a Complete Description of All Single-Point Symmetry-Adapter Perturbation Theory (SAPT) Computations Used in the Present Work (The Units for Energies, Distances, and Angles Are kcal/mol, Å, and Degrees, Respectively.)

	<i>R</i>	3	3	3	3	3	3	3	3	3	3
β_1	45	45	45	45	45	45	90	90	90	90	90
γ_1	0	0	0	60	60	0	0	0	0	0	60
β_2	45	45	45	45	45	0	45	45	45	45	0
α_2	0	45	90	0	45	0	0	45	90	0	0
$E_{\text{int}}^{\text{HF}}$	54.71	76.12	193.89	137.17	160.94	57.99	28.76	21.96	14.37	66.12	
$E_{\text{pol}}^{(10)}$	-27.08	-42.84	125.78	-48.70	-65.44	-39.94	-13.47	-11.21	-10.02	-42.75	
$E_{\text{exch}}^{(10)}$	90.10	129.54	374.04	220.37	263.12	110.20	45.59	36.05	26.76	120.85	
$E_{\text{ind,resp}}^{(20)}$	-43.57	-63.54	229.78	159.27	187.28	-56.29	-21.97	-17.16	-11.58	-57.64	
$E_{\text{exch-ind,resp}}^{(20)}$	35.52	49.65	118.29	99.49	110.77	45.98	20.26	15.93	10.57	46.66	
δ	-0.26	3.30	57.12	25.28	39.77	-1.96	-1.65	-1.65	-1.35	-1.00	
$\epsilon_{\text{pol,resp}}^{(3)}$	-2.40	-1.98	-0.25	-5.54	-4.84	-1.39	-0.72	-0.56	-0.24	-1.48	
$\epsilon_{\text{exch}}^{(1)}(2)$	3.45	2.34	-4.97	-0.93	-2.88	2.65	-0.06	0.29	1.05	2.24	
$'E_{\text{ind}}^{(22)}$	-2.36	-3.38	-9.46	-3.02	-3.76	-3.66	-0.40	-0.46	-0.66	-3.90	
$'E_{\text{exch-ind}}^{(22)}$	1.93	2.64	4.87	1.88	2.22	2.99	0.37	0.42	0.60	3.16	
$E_{\text{disp}}^{(20)}$	-17.54	-21.14	-39.97	-28.49	-31.77	-19.41	-10.48	-9.28	-8.22	-20.42	
$E_{\text{disp}}^{(21)}$	3.87	4.71	10.18	6.22	7.20	6.36	2.95	2.50	2.15	6.44	

Table A-1. The Supplementary Tables Complement Tables 6–10 and Provide a Complete Description of All Single-Point Symmetry-Adapter Perturbation Theory (SAPT) Computations Used in the Present Work (The Units for Energies, Distances, and Angles Are kcal/mol, Å, and Degrees, Respectively.) (continued)

$E_{\text{disp}}^{(22)}$	-3.69	-4.21	-7.10	-5.48	-5.94	-5.08	-2.25	-1.96	-1.88	-5.18
$\varepsilon_{\text{disp}}^{(2)}$	0.18	0.50	3.08	0.74	1.25	1.28	0.71	0.54	0.27	1.26
$E_{\text{disp}}^{(2)}$	-17.36	-20.64	-36.89	-27.75	-30.52	-18.13	-9.77	-8.74	-7.95	-19.16
$E_{\text{exch-disp}}^{(20)}$	3.95	5.03	7.47	5.90	6.71	4.69	2.67	2.24	1.69	4.92
E_{int} E_{corr}	-12.79	-15.99	-39.23	-29.45	-33.06	-12.85	-7.91	-6.80	-5.50	-14.22
E_{int}	41.92	60.12	154.66	107.71	127.88	45.14	20.86	15.16	8.87	51.90
$E_{\text{disp}}^{(20)(+mb)}$	-21.72	-25.87	-45.80	-33.51	-37.17	-23.62	-12.53	-11.20	-9.99	-24.96
$E_{\text{int}}^{(+mb)}$	37.73	55.40	148.83	102.70	122.49	40.92	18.80	13.24	7.10	47.36

Table A-2. Supplementary Tables Continued (For Description and Units, See the Caption of Table A-1.)

R	3	3	3	3	3	3	3	3	3
β_1	90	90	90	135	135	135	135	135	135
γ_1	60	60	60	0	0	0	60	60	60
β_2	45	45	45	45	45	45	45	45	45
α_2	0	45	90	0	45	90	0	45	90
$E_{\text{int}}^{\text{HF}}$	29.31	22.87	16.56	256.62	177.58	84.07	256.98	177.67	84.08
$E_{\text{pol}}^{(1)}$	-13.16	-10.82	-10.23	281.04	166.96	-66.94	280.94	166.89	-66.87
$E_{\text{exch}}^{(10)}$	46.00	36.72	29.22	755.39	438.48	167.01	755.19	438.41	166.96
$E_{\text{ind,resp}}^{(20)}$	-21.64	-16.95	-11.90	556.45	304.55	103.39	556.29	304.49	103.31
$E_{\text{exch-ind,resp}}^{(20)}$	19.87	15.65	10.81	182.22	162.43	80.75	182.22	162.42	80.71
δ	-1.77	-1.72	-1.32	156.50	48.17	6.64	156.80	48.22	6.60
$\varepsilon_{\text{pol,resp}}^{(1)}(3)$	-0.80	-0.67	-0.34	-0.48	0.14	0.88	-0.50	0.13	0.87
$\varepsilon_{\text{exch}}^{(1)}(2)$	0.03	0.36	1.04	-25.15	-13.54	-3.93	-25.15	-13.53	-3.92
$'E_{\text{ind}}^{(22)}$	-0.43	-0.48	-0.72	-15.78	-9.74	-2.55	-15.79	-9.74	-2.55
$'E_{\text{exch-ind}}^{(22)}$	0.39	0.44	0.66	5.17	5.19	1.99	5.17	5.20	1.99
$E_{\text{disp}}^{(20)}$	-10.71	-9.49	-8.55	-61.39	-43.26	-23.43	-61.39	-43.25	-23.43
$E_{\text{disp}}^{(21)}$	2.94	2.49	2.16	26.19	17.10	7.62	26.18	17.09	7.62
$E_{\text{disp}}^{(22)}$	-2.29	-1.99	-1.91	-19.08	-12.01	-5.13	-19.07	-12.01	-5.13
$\varepsilon_{\text{disp}}^{(2)}(2)$	0.66	0.51	0.25	7.11	5.09	2.49	7.11	5.09	2.49

Table A-2. Supplementary Tables Continued (For Description and Units, See the Caption of Table A-1.) (continued)

$E_{\text{disp}}^{(2)}$	-10.05	-8.99	-8.30	-54.28	-38.17	-20.94	-54.28	-38.16	-20.93
$E_{\text{exch-disp}}^{(20)}$	2.68	2.26	1.78	7.58	9.51	7.04	7.58	9.51	7.04
E_{int}	-8.17	-7.08	-5.89	-82.94	-46.60	-17.50	-82.97	-46.61	-17.50
E_{int}	21.14	15.79	10.67	173.68	130.98	66.57	174.01	131.06	66.58
$E_{\text{disp}}^{(20)(+mb)}$	-12.85	-11.51	-10.48	-68.09	-49.89	-28.82	-68.09	-49.89	-28.81
$E_{\text{int}}^{(+mb)}$	19.00	13.77	8.75	166.98	124.34	61.18	167.31	124.42	61.19

Table A-3. Supplementary Tables Continued (For Description and Units, See the Caption of Table A-1.)

R	4	4	4	4	4	4	4	4	4	4
β_1	0	0	0	45	45	45	45	45	45	45
γ_1	0	0	60	0	0	0	0	60	60	60
β_2	0	45	45	0	45	45	45	0	45	45
α_2	0	0	0	0	0	45	90	0	0	45
$E_{\text{int}}^{\text{HF}}$	190.48	49.32	55.37	40.89	5.08	6.44	13.14	103.44	12.31	14.36
$E_{\text{pol}}^{(10)}$	114.28	-28.30	-31.83	-23.76	-1.08	-2.60	-7.87	-57.10	-5.53	-7.34
$E_{\text{exch}}^{(10)}$	335.19	83.96	95.76	69.53	6.72	9.90	23.34	208.96	20.56	25.03
$E_{\text{ind,resp}}^{(20)}$	159.71	-32.21	-39.14	-25.18	-2.08	-3.06	-7.87	130.55	-8.60	-10.47
$E_{\text{exch-ind,resp}}^{(20)}$	88.32	26.80	31.64	21.38	1.81	2.72	6.97	78.09	7.24	8.84
δ	40.95	-0.93	-1.07	-1.09	-0.29	-0.51	-1.43	4.03	-1.36	-1.70
$\epsilon_{\text{pol,resp}}^{(1)}(3)$	-4.30	-1.21	-1.32	-0.83	-0.38	-0.34	-0.37	-1.33	-0.50	-0.45
$\epsilon_{\text{exch}}^{(1)}(2)$	-0.95	2.47	2.55	0.55	0.70	1.31	0.08	0.96	1.05	
$E_{\text{ind}}^{(22)}$	-11.85	-3.02	-3.37	-2.35	-0.18	-0.29	-0.76	-7.67	-0.56	-0.72
$E_{\text{exch-ind}}^{(22)}$	6.55	2.52	2.72	2.00	0.16	0.25	0.67	4.59	0.47	0.61
$E_{\text{disp}}^{(20)}$	-35.39	-13.91	-14.94	-11.85	-3.26	-3.84	-5.90	-23.41	-5.24	-5.83
$E_{\text{disp}}^{(21)}$	9.34	2.67	2.98	2.51	0.55	0.63	1.01	5.71	0.79	0.89
$E_{\text{disp}}^{(22)}$	-6.68	-2.44	-2.64	-2.33	-0.67	-0.77	-1.15	-4.39	-0.97	-1.07

Table A-3. Supplementary Tables Continued. (For Description and Units, See the Caption of Table A-1.) (continued)

$\epsilon_{\text{disp}}^{(2)}$	2.66	0.23	0.34	0.18	-0.12	-0.14	-0.14	1.33	-0.19	-0.17
$E_{\text{disp}}^{(2)}$	-32.74	-13.68	-14.60	-11.67	-3.38	-3.98	-6.04	-22.08	-5.43	-6.01
$E_{\text{exch-disp}}^{(20)}$	5.97	3.17	3.40	2.60	0.42	0.57	1.13	3.46	0.96	1.13
E_{int} ^{corr}	-37.32	-9.76	-10.62	-7.70	-2.82	-3.08	-4.05	-22.95	-4.09	-4.39
E_{int}	153.16	39.57	44.75	33.19	2.26	3.37	9.09	80.49	8.22	9.97
$E_{\text{disp}}^{(20)}(+\text{mb})$	-43.28	-17.02	-18.01	-14.55	-3.92	-3.92	-6.99	-27.02	-6.35	-7.05
$E_{\text{int}}^{(+\text{mb})}$	145.28	36.45	41.68	30.48	1.60	3.29	8.01	76.87	7.11	8.74

Table A-4. Supplementary Tables Continued (For Description and Units, See the Caption of Table A-1.)

R	4	4	4	4	4	4	4	4	4	4	4
β_1	45	90	90	90	90	90	90	90	90	90	135
γ_1	60	0	0	0	0	60	60	60	60	60	0
β_2	45	0	45	45	45	0	45	45	45	45	0
α_2	90	0	0	45	90	0	0	45	90	0	0
$E_{\text{int}}^{\text{HF}}$	22.44	1.95	2.19	1.61	0.41	2.38	2.30	1.75	0.60	22.66	
E_{pol}	-13.79	-1.36	0.94	0.54	-0.42	-1.68	1.08	0.68	-0.41	-11.19	
$E_{\text{exch}}^{(10)}$	42.27	3.72	1.49	1.27	1.00	4.59	1.49	1.30	1.20	37.08	
$E_{\text{ind,resp}}^{(20)}$	-18.32	-1.20	-0.57	-0.47	-0.35	-1.30	-0.57	-0.47	-0.38	-15.25	
$E_{\text{exch-ind,resp}}^{(20)}$	15.20	1.03	0.44	0.36	0.25	1.07	0.41	0.34	0.26	14.08	
δ	-2.92	-0.24	-0.11	-0.09	-0.06	-0.31	-0.12	-0.10	-0.08	-2.07	
$\varepsilon_{\text{pol,resp}}^{(1)}(3)$	-0.37	-0.07	-0.33	-0.23	-0.01	-0.08	-0.36	-0.26	-0.03	-0.86	
$\varepsilon_{\text{exch}}^{(1)}(2)$	1.34	0.34	0.07	0.07	0.09	0.41	0.08	0.08	0.11	1.15	
$E_{\text{ind}}^{(22)}$	-1.35	-0.05	0.01	0.00	-0.01	-0.08	0.01	0.00	-0.01	-1.16	
$E_{\text{exch-ind}}^{(22)}$	1.12	0.04	0.00	0.00	0.00	0.06	0.00	0.00	0.01	1.07	
$E_{\text{disp}}^{(20)}$	-7.96	-2.63	-1.48	-1.40	-1.35	-2.85	-1.53	-1.45	-1.44	-8.19	
$E_{\text{disp}}^{(21)}$	1.33	0.69	0.35	0.33	0.32	0.70	0.35	0.32	0.31	2.52	
$E_{\text{disp}}^{(22)}$	-1.42	-0.67	-0.34	-0.32	-0.32	-0.70	-0.35	-0.32	-0.33	-2.08	
$\varepsilon_{\text{disp}}^{(2)}(2)$	-0.10	0.02	0.01	0.01	0.00	-0.01	0.00	0.00	-0.02	0.44	

Table A-4. Supplementary Tables Continued (For Description and Units, See the Caption of Table A-1.) (continued)

$E_{\text{disp}}^{(2)}$	-8.05	-2.60	-1.47	-1.39	-1.35	-2.86	-1.53	-1.45	-1.46	-7.75
$E_{\text{exch-disp}}^{(2)}$	1.69	0.29	0.13	0.12	0.09	0.32	0.13	0.12	0.10	2.02
$E_{\text{int}}^{\text{corr}}$	-5.62	-2.05	-1.60	-1.44	-1.19	-2.22	-1.67	-1.52	-1.28	-5.53
E_{int}	16.82	-0.09	0.60	0.17	-0.77	0.16	0.63	0.23	-0.68	17.14
$E_{\text{disp}}^{(2)(+\text{mb})}$	-9.50	-3.08	-1.72	-1.63	-1.56	-3.39	-1.78	-1.70	-1.68	-10.07
$E_{\text{int}}^{(+\text{mb})}$	15.27	-0.54	0.36	-0.06	-0.98	-0.37	0.38	-0.01	-0.92	15.25

Table A-5. Supplementary Tables Continued (For Description and Units, See the Caption of Table A-1.)

R	4	4	4	4	4	4	4	4	4
β_1	135	135	135	135	135	135	135	180	180
γ_1	0	0	0	60	60	60	0	0	60
β_2	45	45	45	0	45	45	0	45	45
a_2	0	45	90	0	0	45	90	0	0
$E_{\text{int}}^{\text{HF}}$	15.89	11.39	5.11	22.59	15.88	11.39	5.11	193.11	34.87
$E_{\text{pol}}^{(10)}$	-5.79	-4.28	-2.94	-11.16	-5.78	-4.26	-2.92	116.65	-21.29
$E_{\text{exch}}^{(10)}$	23.87	17.30	8.91	36.99	23.85	17.29	8.89	335.28	60.58
$E_{\text{ind,resp}}^{(20)}$	-9.00	-6.48	-3.39	-15.20	-8.99	-6.48	-3.39	187.58	-26.46
$E_{\text{exch-ind,resp}}^{(20)}$	8.27	5.97	3.10	14.04	8.27	5.96	3.09	103.24	23.14
δ	-1.46	-1.12	-0.57	-2.08	-1.47	-1.12	-0.57	58.83	-1.11
$\varepsilon_{\text{pol,resp}}^{(1)}(3)$	-0.99	-0.71	-0.27	-0.86	-0.99	-0.72	-0.27	-3.86	-1.58
$\varepsilon_{\text{exch}}^{(1)}(2)$	1.49	1.08	0.49	1.15	1.49	1.08	0.49	-4.31	1.87
$'E_{\text{ind}}^{(22)}$	-1.14	-0.75	-0.28	-1.16	-1.14	-0.75	-0.28	-11.92	-3.32
$'E_{\text{exch-ind}}^{(22)}$	1.05	0.69	0.26	1.07	1.05	0.69	0.26	6.56	2.90
$E_{\text{disp}}^{(20)}$	-6.09	-5.08	-3.50	-8.18	-6.09	-5.08	-3.50	-31.23	-10.53
$E_{\text{disp}}^{(21)}$	1.89	1.49	0.90	2.52	1.89	1.49	0.90	11.49	3.19
$E_{\text{disp}}^{(22)}$	-1.83	-1.42	-0.84	-2.08	-1.83	-1.42	-0.84	-9.11	-2.95
$\varepsilon_{\text{disp}}^{(2)}$	0.06	0.06	0.06	0.44	0.06	0.06	0.06	2.38	0.24

Table A-5. Supplementary Tables Continued (For Description and Units, See the Caption of Table A-1.) (continued)

$E_{\text{disp}}^{(2)}$	-6.03	-5.02	-3.44	-7.75	-6.03	-5.02	-3.44	-28.86	-10.29	-10.29
$E_{\text{exch-disp}}^{(2)}$	1.38	1.09	0.65	2.02	1.38	1.09	0.65	6.12	2.83	2.83
E_{int} ^{corr}	-4.24	-3.62	-2.59	-5.53	-4.24	-3.62	-2.59	-36.26	-7.59	-7.59
E_{int}	11.65	7.77	2.52	17.06	11.64	7.77	2.52	156.85	27.28	27.29
$E_{\text{disp}}^{(2)(+\text{mb})}$	-7.14	-6.01	-4.22	-10.07	-7.14	-6.01	-4.22	-38.61	-13.03	-13.03
$E_{\text{int}}^{(+\text{mb})}$	10.59	6.84	1.80	15.17	10.58	6.83	1.80	149.48	24.78	24.78

Table A-6. Supplementary Tables Continued (For Description and Units, See the Caption of Table A-1.)

	R	5	5	5	5	5	5	5	5	5	5
β_1	0	0	0	45	45	45	45	45	45	45	45
γ_1	0	0	60	0	0	0	0	60	60	60	60
β_2	0	45	45	0	45	45	45	0	45	45	45
α_2	0	0	0	0	0	45	90	0	0	45	45
$E_{\text{int}}^{\text{HF}}$	5.14	1.27	1.35	0.77	0.50	0.38	0.20	2.79	0.64	0.60	
$E_{\text{pol}}^{(10)}$	-3.90	-1.01	-1.05	-1.50	0.25	0.04	-0.45	-3.59	-0.15	-0.33	
$E_{\text{exch}}^{(10)}$	9.87	2.56	2.69	2.55	0.31	0.42	0.79	7.49	1.00	1.16	
$E_{\text{ind,resp}}^{(20)}$	-2.23	-0.62	-0.67	-0.61	-0.10	-0.13	-0.22	-2.36	-0.31	-0.35	
$E_{\text{exch-ind,resp}}^{(20)}$	1.92	0.49	0.53	0.48	0.05	0.07	0.14	1.90	0.20	0.23	
δ	-0.53	-0.14	-0.15	-0.15	-0.02	-0.03	-0.06	-0.65	-0.09	-0.11	
$\varepsilon_{\text{pol,resp}}^{(1)}(3)$	-0.12	-0.04	-0.05	0.07	-0.08	-0.05	0.01	0.04	-0.06	-0.04	
$\varepsilon_{\text{exch}}^{(1)}(2)$	1.16	0.34	0.35	0.34	0.05	0.06	0.11	0.76	0.11	0.13	
$tE_{\text{ind}}^{(22)}$	-0.38	-0.09	-0.09	-0.07	0.00	-0.01	-0.02	-0.25	-0.02	-0.03	
$tE_{\text{exch-ind}}^{(22)}$	0.33	0.07	0.07	0.06	0.00	0.00	0.01	0.20	0.01	0.02	
$E_{\text{disp}}^{(20)}$	-3.75	-1.78	-1.82	-1.69	-0.66	-0.72	-0.92	-2.66	-0.93	-0.99	
$E_{\text{disp}}^{(21)}$	0.66	0.26	0.26	0.30	0.11	0.12	0.14	0.44	0.12	0.13	
$E_{\text{disp}}^{(22)}$	-0.80	-0.37	-0.38	-0.40	-0.15	-0.16	-0.21	-0.59	-0.20	-0.21	
$\varepsilon_{\text{disp}}^{(2)}(2)$	-0.14	-0.12	-0.11	-0.10	-0.04	-0.04	-0.06	-0.15	-0.08	-0.08	

Table A-6. Supplementary Tables Continued (For Description and Units, See the Caption of Table A-1.) (continued)

$E_{\text{disp}}^{(2)}$	-3.89	-1.90	-1.93	-1.78	-0.69	-0.77	-0.98	-2.81	-1.01	-1.07
$E_{\text{exch-disp}}^{(20)}$	0.52	0.17	0.17	0.16	0.02	0.03	0.06	0.40	0.06	0.07
$E_{\text{int}}^{\text{corr}}$	-2.39	-1.45	-1.47	-1.23	-0.70	-0.73	-0.81	-1.67	-0.90	-0.92
E_{int}	2.75	-0.18	-0.12	-0.46	-0.20	-0.35	-0.61	1.12	-0.26	-0.31
$E_{\text{disp}}^{(20)(+\text{mb})}$	-4.55	-2.09	-2.13	-1.96	-0.74	-0.82	-1.04	-3.11	-1.06	-1.13
$E_{\text{int}}^{(+\text{mb})}$	1.95	-0.49	-0.43	-0.73	-0.29	-0.44	-0.73	0.68	-0.39	-0.46

Table A-7. Supplementary Tables Continued (For Description and Units, See the Caption of Table A-1.)

R	5	5	5	5	5	5	5	5	5
β_1	45	90	90	90	90	90	90	90	90
γ_1	60	0	0	0	60	60	60	60	0
β_2	45	0	45	45	0	45	45	45	0
α_2	90	0	0	45	90	0	0	45	90
$E_{\text{int}}^{\text{HF}}$	0.57	-0.03	0.65	0.44	-0.04	-0.09	0.68	0.48	-0.03
$E_{\text{pol}}^{(10)}$	-0.82	-0.09	0.64	0.43	-0.04	-0.17	0.68	0.47	-0.04
$E_{\text{exch}}^{(10)}$	1.69	0.10	0.04	0.04	0.03	0.13	0.04	0.04	0.04
$E_{\text{ind,resp}}^{(20)}$	-0.49	-0.06	-0.04	-0.04	-0.03	-0.07	-0.04	-0.04	-0.03
$E_{\text{exch-ind,resp}}^{(20)}$	0.35	0.02	0.01	0.01	0.02	0.01	0.01	0.01	0.30
δ	-0.15	-0.01	0.00	0.00	-0.01	0.00	0.00	0.00	-0.09
$\varepsilon_{\text{pol,resp}}^{(1)}(3)$	0.02	0.00	-0.14	-0.10	0.00	0.01	-0.15	-0.10	0.00
$\varepsilon_{\text{exch}}^{(1)}(2)$	0.19	0.01	0.00	0.00	0.00	0.02	0.00	0.00	0.17
$'E_{\text{ind}}^{(22)}$	-0.05	0.01	0.00	0.00	0.00	0.01	0.01	0.00	-0.03
$'E_{\text{exch-ind}}^{(22)}$	0.03	0.00	0.00	0.00	0.00	0.00	0.00	0.00	0.02
$E_{\text{disp}}^{(20)}$	-1.18	-0.50	-0.32	-0.31	-0.31	-0.54	-0.33	-0.32	-1.16
$E_{\text{disp}}^{(21)}$	0.15	0.14	0.08	0.08	0.14	0.08	0.08	0.08	0.33
$E_{\text{disp}}^{(22)}$	-0.25	-0.14	-0.08	-0.08	-0.15	-0.08	-0.08	-0.08	-0.34
$\varepsilon_{\text{disp}}^{(2)}(2)$	-0.10	0.00	0.00	0.00	-0.01	0.00	0.00	0.00	-0.02

Table A-7. Supplementary Tables Continued (For Description and Units, See the Caption of Table A-1.) (continued)

$E_{\text{disp}}^{(2)}$	-1.28	-0.50	-0.32	-0.31	-0.31	-0.55	-0.33	-0.32	-0.33	-1.18
$E_{\text{exch-disp}}^{(20)}$	0.10	0.01	0.00	0.00	0.00	0.01	0.00	0.00	0.00	0.11
$E_{\text{int}}^{\text{corr}}$	-0.98	-0.47	-0.44	-0.39	-0.29	-0.51	-0.46	-0.41	-0.32	-1.16
E_{int}	-0.41	-0.50	0.21	0.05	-0.33	-0.60	0.22	0.06	-0.35	0.48
$E_{\text{disp}}^{(20)(+\text{mb})}$	-1.35	-0.55	-0.35	-0.34	-0.33	-0.60	-0.36	-0.35	-0.36	-1.34
$E_{\text{int}}^{(+\text{mb})}$	-0.59	-0.55	,0.18	0.02	-0.36	-0.66	0.19	0.03	-0.38	0.29

Table A-8. Supplementary Tables Continued (For Description and Units, See the Caption of Table A-1.)

R	5	5	5	5	5	5	5	5	5
β_1	135	135	135	135	135	135	135	180	180
γ_1	0	0	0	60	60	60	0	0	60
β_2	45	45	45	0	45	45	0	45	45
α_2	0	45	90	0	0	45	90	0	0
$E_{\text{int}}^{\text{HF}}$	1.37	1.03	0.33	1.63	1.37	1.03	0.33	7.51	1.58
$E_{\text{pol}}^{(10)}$	0.92	0.67	0.10	0.64	0.92	0.67	0.10	-0.47	-0.04
$E_{\text{exch}}^{(10)}$	0.63	0.52	0.33	1.23	0.63	0.52	0.33	8.86	1.96
$E_{\text{ind,resp}}^{(20)}$	-0.27	-0.23	-0.15	-0.44	-0.27	-0.23	-0.15	-2.73	-0.66
$E_{\text{exch-ind,resp}}^{(20)}$	0.13	0.11	0.07	0.30	0.13	0.11	0.07	2.33	0.43
δ	-0.04	-0.03	-0.02	-0.09	-0.04	-0.03	-0.02	-0.49	-0.11
$\epsilon_{\text{pol,resp}}^{(1)}(3)$	-0.21	-0.16	-0.07	-0.25	-0.21	-0.16	-0.07	-0.74	-0.21
$\epsilon_{\text{exch}}^{(1)}(2)$	0.11	0.09	0.05	0.17	0.11	0.09	0.05	1.15	0.33
$tE_{\text{ind}}^{(22)}$	-0.02	-0.02	0.00	-0.03	-0.02	-0.02	0.00	-0.57	-0.13
$tE_{\text{exch-ind}}^{(22)}$	0.01	0.01	0.00	0.02	0.01	0.01	0.00	0.49	0.09
$E_{\text{disp}}^{(20)}$	-0.82	-0.74	-0.60	-1.16	-0.82	-0.74	-0.60	-3.12	-1.38
$E_{\text{disp}}^{(21)}$	0.24	0.21	0.15	0.33	0.24	0.21	0.15	0.93	0.36
$E_{\text{disp}}^{(22)}$	-0.28	-0.24	-0.17	-0.34	-0.28	-0.24	-0.17	-1.08	-0.45
$\epsilon_{\text{disp}}^{(2)}(2)$	-0.04	-0.03	-0.01	-0.02	-0.04	-0.03	-0.01	-0.15	-0.08

Table A-8. Supplementary Tables Continued (For Description and Units, See the Caption of Table A-1.) (continued)

$E_{\text{disp}}^{(2)}$	-0.86	-0.77	-0.61	-1.18	-0.86	-0.77	-0.61	-3.27	-1.46	-1.46
$E_{\text{exch-disp}}^{(2)}$	0.05	0.05	0.03	0.11	0.05	0.05	0.03	0.56	0.15	0.15
E_{int} ^{corr}	-0.91	-0.81	-0.60	-1.16	-0.91	-0.81	-0.60	-2.38	-1.23	-1.23
E_{int}	0.45	0.22	-0.28	0.47	0.46	0.22	-0.27	5.13	0.35	0.35
$E_{\text{disp}}^{(2)(+\text{mb})}$	-0.94	-0.85	-0.69	-1.34	-0.94	-0.85	-0.69	-3.71	-1.60	-1.60
$E_{\text{int}}^{(+\text{mb})}$	0.34	0.11	-0.37	0.29	0.34	0.11	-0.37	4.54	0.12	0.12

Table A-9. Supplementary Tables Continued (For Description and Units, See the Caption of Table A-1.)

R	6	6	6	6	6	6	6	6	6
β_1	0	0	0	45	45	45	45	45	45
γ_1	0	0	60	0	0	0	60	60	60
β_2	0	45	45	0	45	45	0	45	45
α_2	0	0	0	0	0	45	90	0	45
$E_{\text{int}}^{\text{HF}}$	-0.54	-0.15	-0.15	-0.43	0.14	0.05	-0.13	-0.54	0.07
$E_{\text{pol}}^{(10)}$	-0.67	-0.17	-0.17	-0.45	0.14	0.06	-0.12	-0.65	0.06
$E_{\text{exch}}^{(10)}$	0.20	0.06	0.06	0.06	0.01	0.01	0.02	0.18	0.03
$E_{\text{ind,resp}}^{(20)}$	-0.08	-0.04	-0.04	-0.04	-0.02	-0.02	-0.02	-0.08	-0.03
$E_{\text{exch-ind,resp}}^{(20)}$	0.02	0.01	0.01	0.01	0.00	0.00	0.00	0.03	0.00
δ	-0.01	0.00	0.00	-0.01	0.00	0.00	0.00	-0.01	-0.01
$\varepsilon_{\text{pol,resp}}^{(1)}(3)$	0.12	0.03	0.03	0.08	-0.03	-0.01	0.02	0.10	-0.02
$\varepsilon_{\text{exch}}^{(1)}(2)$	0.05	0.01	0.01	0.02	0.00	0.00	0.00	0.04	0.01
$'E_{\text{ind}}^{(22)}$	0.00	0.00	0.00	0.00	0.00	0.00	0.00	0.00	0.00
$'E_{\text{exch-ind}}^{(22)}$	0.00	0.00	0.00	0.00	0.00	0.00	0.00	0.00	0.00
$E_{\text{disp}}^{(20)}$	-0.58	-0.34	-0.34	-0.33	-0.17	-0.18	-0.21	-0.43	-0.21
$E_{\text{disp}}^{(21)}$	0.11	0.06	0.06	0.07	0.03	0.04	0.04	0.08	0.03
$E_{\text{disp}}^{(22)}$	-0.15	-0.08	-0.08	-0.09	-0.04	-0.04	-0.05	-0.12	-0.05
$\varepsilon_{\text{disp}}^{(2)}(2)$	-0.04	-0.02	-0.02	-0.02	-0.01	-0.01	-0.01	-0.04	-0.02

Table A-9. Supplementary Tables Continued (For Description and Units, See the Caption of Table A-1.) (continued)

$E_{\text{disp}}^{(2)}$	-0.62	-0.36	-0.36	-0.35	-0.18	-0.19	-0.22	-0.47	-0.23	-0.24
$E_{\text{exch-disp}}^{(20)}$	0.02	0.01	0.01	0.01	0.00	0.00	0.00	0.01	0.00	0.00
E_{int} ^{corr}	-0.44	-0.31	-0.31	-0.25	-0.20	-0.20	-0.19	-0.31	-0.23	-0.23
E_{int}	-0.98	-0.46	-0.46	-0.68	-0.07	-0.14	-0.32	-0.85	-0.17	-0.23
$E_{\text{disp}}^{(20)(+\text{mb})}$	-0.64	-0.37	-0.37	-0.36	-0.18	-0.19	-0.22	-0.46	-0.23	-0.23
$E_{\text{int}}^{(+\text{mb})}$	-1.04	-0.49	-0.49	-0.71	-0.08	-0.16	-0.33	-0.89	-0.18	-0.24

Table A-10. Supplementary Tables Continued (For Description and Units, See the Caption of Table A-1.)

R	6	6	6	6	6	6	6	6	6	6	6
β_1	45	90	90	90	90	90	90	90	90	90	90
γ_1	60	0	0	0	0	0	60	60	60	60	0
β_2	45	0	45	45	45	0	45	45	45	45	0
α_2	90	0	0	45	90	0	0	45	90	0	0
$E_{\text{int}}^{\text{HF}}$	-0.15	-0.04	0.32	0.22	-0.02	-0.07	0.34	0.23	-0.02	0.50	
$E_{\text{pol}}^{(10)}$	-0.16	-0.03	0.33	0.23	-0.02	-0.06	0.34	0.24	-0.02	0.51	
$E_{\text{exch}}^{(10)}$	0.05	0.00	0.00	0.00	0.00	0.00	0.00	0.00	0.00	0.03	
$E_{\text{ind, resp}}^{(20)}$	-0.03	-0.01	-0.01	-0.01	-0.01	-0.01	-0.01	-0.01	-0.01	-0.05	
$E_{\text{exch-ind, resp}}^{(20)}$	0.01	0.00	0.00	0.00	0.00	0.00	0.00	0.00	0.00	0.01	
δ	-0.01	0.00	0.00	0.00	0.00	0.00	0.00	0.00	0.00	0.00	
$\varepsilon_{\text{pol, resp}}^{(1)}(3)$	0.03	0.00	-0.07	-0.05	0.00	0.01	-0.07	-0.05	0.00	-0.10	
$\varepsilon_{\text{exch}}^{(1)}(2)$	0.01	0.00	0.00	0.00	0.00	0.00	0.00	0.00	0.00	0.01	
$E_{\text{ind}}^{(22)}$	0.00	0.00	0.00	0.00	0.00	0.00	0.00	0.00	0.00	0.00	
$E_{\text{exch-ind}}^{(22)}$	0.00	0.00	0.00	0.00	0.00	0.00	0.00	0.00	0.00	0.00	
$E_{\text{disp}}^{(20)}$	-0.24	-0.14	-0.10	-0.09	-0.09	-0.15	-0.10	-0.10	-0.10	-0.24	
$E_{\text{disp}}^{(21)}$	0.04	0.04	0.03	0.02	0.03	0.04	0.03	0.02	0.03	0.08	
$E_{\text{disp}}^{(22)}$	-0.06	-0.04	-0.03	-0.02	-0.02	-0.04	-0.03	-0.02	-0.03	-0.08	
$\varepsilon_{\text{disp}}^{(2)}(2)$	-0.02	0.00	0.00	0.00	0.00	0.00	0.00	0.00	0.00	-0.01	

Table A-10. Supplementary Tables Continued (For Description and Units, See the Caption of Table A-1.) (continued)

$E_{\text{disp}}^{(2)}$	-0.26	-0.14	-0.09	-0.09	-0.09	-0.15	-0.10	-0.10	-0.10	-0.25
$E_{\text{exch-disp}}^{(20)}$	0.00	0.00	0.00	0.00	0.00	0.00	0.00	0.00	0.00	0.00
E_{int}	-0.22	-0.13	-0.16	-0.14	-0.09	-0.14	-0.17	-0.14	-0.10	-0.34
E_{int}	-0.37	-0.17	0.16	0.08	-0.11	-0.21	0.17	0.09	-0.12	0.16
$E_{\text{disp}}^{(20)(+\text{mb})}$	-0.26	-0.14	-0.10	-0.10	-0.10	-0.15	-0.10	-0.10	-0.10	-0.26
$E_{\text{int}}^{(+\text{mb})}$	-0.39	-0.18	0.16	0.08	-0.12	-0.22	0.16	0.08	-0.12	0.14

Table A-11. Supplementary Tables Continued (For Description and Units, See the Caption of Table A-1.)

R	6	6	6	6	6	6	6	6	6	6	6
β_1	135	135	135	135	135	135	135	135	180	180	180
γ_1	0	0	0	60	60	60	60	60	0	0	60
β_2	45	45	45	0	45	45	45	45	0	45	45
α_2	0	45	90	0	0	45	90	0	0	0	0
$E_{\text{int}}^{\text{HF}}$	0.48	0.36	0.09	0.50	0.48	0.36	0.09	0.09	1.07	0.23	0.23
$E_{\text{pol}}^{(10)}$	0.51	0.38	0.11	0.51	0.51	0.39	0.11	0.99	0.24	0.24	0.24
$E_{\text{exch}}^{(10)}$	0.02	0.01	0.01	0.03	0.02	0.01	0.01	0.20	0.05	0.05	0.05
$E_{\text{ind,resp}}^{(20)}$	-0.04	-0.04	-0.03	-0.05	-0.04	-0.04	-0.03	-0.15	-0.07	-0.07	-0.07
$E_{\text{exch-ind,resp}}^{(20)}$	0.00	0.00	0.00	0.01	0.00	0.00	0.00	0.03	0.01	0.01	0.01
δ	0.00	0.00	0.00	0.00	0.00	0.00	0.00	0.00	0.00	0.00	0.00
$\epsilon_{\text{pol,resp}}^{(1)}(3)$	-0.08	-0.07	-0.03	-0.10	-0.08	-0.07	-0.03	-0.17	-0.05	-0.05	-0.05
$\epsilon_{\text{exch}}^{(1)}(2)$	0.00	0.00	0.00	0.01	0.00	0.00	0.00	0.06	0.02	0.02	0.02
$'E_{\text{ind}}^{(22)}$	0.00	0.00	0.00	0.00	0.00	0.00	0.00	-0.01	0.00	0.00	0.00
$'E_{\text{exch-ind}}^{(22)}$	0.00	0.00	0.00	0.00	0.00	0.00	0.00	0.00	0.00	0.00	0.00
$E_{\text{disp}}^{(20)}$	-0.18	-0.17	-0.15	-0.24	-0.18	-0.17	-0.15	-0.48	-0.27	-0.27	-0.27
$E_{\text{disp}}^{(21)}$	0.06	0.05	0.04	0.08	0.06	0.05	0.04	0.16	0.08	0.08	0.08
$E_{\text{disp}}^{(22)}$	-0.07	-0.06	-0.05	-0.08	-0.07	-0.06	-0.05	-0.20	-0.10	-0.10	-0.10
$\epsilon_{\text{disp}}^{(2)}(2)$	-0.01	-0.01	0.00	-0.01	-0.01	-0.01	0.00	-0.04	-0.02	-0.02	-0.02

Table A-11. Supplementary Tables Continued (For Description and Units, See the Caption of Table A-1.) (continued)

$E_{\text{disp}}^{(2)}$	-0.19	-0.18	-0.15	-0.25	-0.19	-0.18	-0.15	-0.51	-0.28	-0.28
$E_{\text{exch-disp}}^{(2)}$	0.00	0.00	0.00	0.00	0.00	0.00	0.00	0.02	0.00	0.00
$E_{\text{int}}^{\text{corr}}$	-0.27	-0.24	-0.17	-0.34	-0.27	-0.24	-0.17	-0.61	-0.31	-0.31
E_{int}	0.21	0.12	-0.08	0.16	0.21	0.12	-0.08	0.45	-0.08	-0.08
$E_{\text{disp}}^{(2)(+\text{mb})}$	-0.20	-0.19	-0.16	-0.26	-0.20	-0.19	-0.16	-0.52	-0.29	-0.29
$E_{\text{int}}^{(+\text{mb})}$	0.20	0.11	-0.09	0.14	0.20	0.11	-0.09	0.40	-0.11	-0.11

Table A-12. Supplementary Tables Continued (For Description and Units, See the Caption of Table A-1.)

R	3.33 ^a	3.33	3.33	3.33	3.33	3.33	3.50	3.50	3.50	3.50
β_1	135	90	45	45	180	135	90	45	45	180
γ_1	60.15 ^b	60.15	60.15	0.15 ^c	0.15	60.15	60.15	0.15	0.15	0.15
β_2	116.67	116.67	116.67	116.67	116.67	116.67	116.67	116.67	116.67	116.67
α_2	359.98	359.98	359.98	359.98	359.98	359.98	359.98	359.98	359.98	359.98
$E_{\text{int}}^{\text{HF}}$	4.04	5.40	163.58	101.09	82.56	1.39	2.15	97.75	58.89	0.23
$E_{\text{pol}}^{(10)}$	-8.47	-6.71	-93.18	-60.46	-70.35	-5.85	-4.36	-56.06	-34.04	-2.44
$E_{\text{exch}}^{(10)}$	14.22	14.19	300.97	172.72	168.33	8.33	7.73	178.44	99.29	3.13
$E_{\text{ind,resp}}^{(20)}$	-7.71	-4.76	-194.21	-80.67	-100.25	-4.38	-2.47	-102.66	-41.41	-1.05
$E_{\text{exch-ind,resp}}^{(20)}$	6.52	3.81	107.01	58.81	73.29	3.63	1.88	69.11	33.77	0.75
δ	-0.54	-1.13	42.99	10.70	11.56	-0.34	-0.62	8.92	1.28	-0.17
$\varepsilon_{\text{pol,resp}}^{(1)}(3)$	0.44	0.22	-0.90	-1.25	-2.09	0.40	0.25	-0.94	-1.03	0.26
$\varepsilon_{\text{exch}}^{(1)}(2)$	0.68	1.00	-4.09	0.42	1.10	0.46	0.65	-0.54	1.67	0.35
$E_{\text{ind}}^{(22)}$	-0.06	-0.40	-7.84	-5.38	-7.41	-0.02	-0.20	-5.10	-3.27	-0.07
$E_{\text{exch-ind}}^{(22)}$	0.05	0.32	4.32	3.92	5.41	0.02	0.16	3.43	2.67	0.05
$E_{\text{disp}}^{(20)}$	-5.55	-4.90	-31.98	-22.33	-22.56	-4.02	-3.47	-21.74	-15.22	-2.59
$E_{\text{disp}}^{(21)}$	1.48	0.97	7.38	4.77	7.09	1.04	0.67	4.54	2.95	0.58

^a Unless otherwise noted, the full value of the coordinates are given in Table 2 for the G1 geometry.

^b Full coordinate value is 60.147002.

^c Full coordinate value is 0.147002.

Table A-12. Supplementary Tables Continued (For Description and Units, See the Caption of Table A-1.) (continued)

$E_{\text{disp}}^{(22)}$	-1.43	-1.10	-5.22	-3.79	-5.97	-1.03	-0.80	-3.60	-2.63	-0.65
$\varepsilon_{\text{disp}}^{(2)}(2)$	0.04	-0.13	2.16	0.98	1.12	0.01	-0.13	0.94	0.32	-0.07
$E_{\text{disp}}^{(2)}(2)$	-5.51	-5.03	-29.82	-21.35	-21.44	-4.01	-3.59	-20.79	-14.89	-2.66
$E_{\text{exch-disp}}^{(20)}$	1.01	0.73	6.20	5.29	6.25	0.63	0.43	4.79	3.61	0.23
E_{int}	-3.39	-3.16	-32.12	-18.34	-18.17	-2.52	-2.30	-19.15	-11.24	-1.84
E_{int}	0.64	2.24	131.45	82.75	64.39	-1.14	-0.15	78.60	-47.66	-1.61
$E_{\text{disp}}^{(20)(+mb)}$	-6.74	-5.59	-35.71	-25.62	-27.46	-4.86	-3.95	-24.65	-17.69	-2.95
$E_{\text{int}}^{(+mb)}$	-0.55	1.55	-127.72	79.46	59.49	-1.97	-0.64	75.69	45.19	-1.98

^a Unless otherwise noted, the full value of the coordinates are given in Table 2 for the G1 geometry.

^b Full coordinate value is 60.147002.

^c Full coordinate value is 0.147002.

Table A-13. Supplementary Tables Continued (For Description and Units, See the Caption of Table A-1; See Footnotes in Table A-12 for Coordinate Information.)

R	3.50	3.50	3.75	3.75	3.75	3.75	3.75	3.75	3.75	3.75
β_1	135	180	135	90	45	0	45	90	135	180
γ_1	0.15	0.15	60.15	60.15	60.15	0.15	0.15	0.15	0.15	0.15
β_2	116.67	116.67	116.67	116.67	116.67	116.67	116.67	116.67	116.67	116.67
α_2	359.98	359.98	359.98	359.98	359.98	359.98	359.98	359.98	359.98	359.98
$E_{\text{int}}^{\text{HF}}$	1.48	50.13	-0.43	0.02	44.82	41.21	26.02	-0.59	-0.36	22.76
$E_{\text{pol}}^{(10)}$	-5.83	-41.68	-3.64	-2.55	-25.36	-21.02	-14.53	-1.59	-3.62	-19.28
$E_{\text{exch}}^{(10)}$	8.39	99.54	3.81	3.17	80.44	66.92	43.36	1.26	3.84	45.29
$E_{\text{ind, resp}}^{(20)}$	-4.41	-53.55	-1.96	-0.99	-39.05	-25.77	-15.36	-0.47	-1.97	-21.01
$E_{\text{exch-ind, resp}}^{(20)}$	3.67	43.20	1.54	0.66	30.97	21.95	13.66	0.28	1.55	18.26
δ	-0.34	2.62	-0.17	-0.27	-2.18	-0.88	-1.11	-0.07	-0.17	-0.50
$\varepsilon_{\text{pol, resp}}^{(1)}(3)$	0.40	-1.64	0.35	0.26	-0.72	-1.47	-0.63	0.24	0.34	-1.02
$\varepsilon_{\text{exch}}^{(1)}(2)$	0.46	2.17	0.25	0.33	1.31	2.45	1.69	0.17	0.25	2.15
$E_{\text{ind}}^{(22)}$	-0.02	-5.02	0.00	-0.07	-2.48	-2.28	-1.49	-0.02	0.00	-2.61
$E_{\text{exch-ind}}^{(22)}$	0.02	4.05	0.00	0.05	1.97	1.94	1.32	0.01	0.00	2.27
$E_{\text{disp}}^{(20)}$	-4.01	-15.74	-2.55	-2.15	-12.36	-12.73	-8.78	-1.66	-2.55	-9.34
$E_{\text{disp}}^{(21)}$	1.04	4.71	0.64	0.41	2.22	2.21	1.49	0.37	0.64	2.60
$E_{\text{disp}}^{(22)}$	-1.03	-4.21	-0.65	-0.51	-2.10	-2.26	-1.57	-0.43	-0.65	-2.55

Table A-13. Supplementary Tables Continued (For Description and Units, See the Caption of Table A-1; See Footnotes in Table A-12 for Coordinate Information.) (continued)

$\varepsilon_{\text{disp}}^{(2)}$	0.01	0.49	-0.01	-0.10	0.11	-0.06	-0.07	-0.05	-0.01	0.05
$E_{\text{disp}}^{(2)}$	-4.00	-15.25	-2.56	-2.25	-12.25	-12.79	-8.85	-1.71	-2.56	-9.29
$E_{\text{exch-disp}}^{(20)}$	0.63	4.33	0.31	0.20	2.82	2.82	1.92	0.10	0.31	2.38
E_{int} ^{corr}	-2.52	-11.36	-1.66	-1.49	-9.35	-9.32	-6.04	-1.21	-1.65	-6.12
E_{int}	-1.04	38.78	-2.08	-1.47	35.47	31.89	19.98	-1.80	-2.01	16.65
$E_{\text{disp}}^{(20)(+\text{mb})}$	-4.85	-19.26	-3.05	-2.43	-14.28	-16.74	-10.31	-1.87	-3.05	-11.41
$E_{\text{int}}^{(+\text{mb})}$	-1.87	35.26	-2.59	-1.75	33.55	27.87	18.45	-2.01	-2.52	14.57

Table A-14. Supplementary Tables Continued (For Description and Units, See the Caption of Table A-1; See Footnotes in Table A-12 for Coordinate Information.)

R	4.00	4.00	4.00	4.25	4.25	4.25	4.25	4.25	4.25
β_1	135	90	45	135	90	45	0	45	90
γ_1	60.15	60.15	60.15	60.15	60.15	60.15	0.15	0.15	0.15
β_2	116.67	116.67	116.67	116.67	116.67	116.67	116.67	116.67	116.67
α_2	359.98	359.98	359.98	359.98	359.98	359.98	359.98	359.98	359.98
$E_{\text{int}}^{\text{HF}}$	-1.05	-0.69	19.82	-1.17	-0.84	8.47	8.21	4.47	-0.78
$E_{\text{pol}}^{(10)}$	-2.44	-1.65	-11.03	-1.74	-1.17	-4.69	-3.39	-2.61	-0.88
$E_{\text{exch}}^{(10)}$	1.73	1.28	35.01	0.78	0.51	14.86	12.64	7.71	0.20
$E_{\text{ind,resp}}^{(20)}$	-0.90	-0.43	-14.51	-0.43	-0.21	-5.37	-3.67	-2.10	-0.12
$E_{\text{exch-ind,resp}}^{(20)}$	0.64	0.23	12.37	0.26	0.08	4.64	3.25	1.89	0.04
δ	-0.08	0.11	-2.02	-0.04	-0.05	-0.97	-0.62	-0.41	-0.01
$\varepsilon_{\text{pol,resp}}^{(1)}(3)$	0.29	0.24	-0.44	0.24	0.20	-0.23	-0.48	-0.14	0.18
$\varepsilon_{\text{exch}}^{(1)}(2)$	0.13	0.16	1.31	0.07	0.07	0.87	1.02	0.64	0.03
$tE_{\text{ind}}^{(22)}$	0.01	-0.02	-1.12	0.01	-0.01	-0.48	-0.43	-0.26	0.00
$tE_{\text{exch-ind}}^{(22)}$	-0.01	0.01	0.95	-0.01	0.00	0.41	0.38	0.23	0.00
$E_{\text{disp}}^{(20)}$	-1.64	-1.37	-7.07	-1.08	-0.89	-4.11	-4.52	-3.06	-0.73
$E_{\text{disp}}^{(21)}$	0.41	0.27	1.09	0.27	0.18	0.56	0.64	0.43	0.17
$E_{\text{disp}}^{(22)}$	-0.42	-0.34	-1.24	-0.28	-0.23	-0.75	-0.85	-0.59	-0.20

Table A-14. Supplementary Tables Continued (For Description and Units, See the Caption of Table A-1; See Footnotes in Table A-12 for Coordinate Information.) (continued)

$\varepsilon_{\text{disp}}^{(2)}$	-0.01	-0.07	-0.15	-0.01	-0.05	-0.19	-0.21	-0.16	-0.02	0.00
$E_{\text{disp}}^{(2)}$	-1.66	-1.44	-7.22	-1.09	-0.94	-4.30	-4.73	-3.22	-0.75	-0.75
$E_{\text{exch-disp}}^{(20)}$	0.15	0.09	1.49	0.07	0.04	0.73	0.70	0.44	0.02	0.03
$E_{\text{int}}^{\text{corr}}$	-1.08	-0.97	-5.03	-0.71	-0.63	-3.00	-3.55	-2.31	-0.52	-0.45
E_{int}	-2.14	-1.66	14.79	-1.88	-1.47	5.47	4.66	2.17	-1.29	-1.54
$E_{\text{disp}}^{(20)(+\text{mb})}$	-1.95	-1.53	-8.28	-1.27	-0.99	-4.82	-5.70	-3.58	-0.81	-1.27
$E_{\text{int}}^{(+\text{mb})}$	-2.44	-1.83	13.59	-2.07	-1.57	4.76	3.47	1.64	-1.37	-2.06

Table A-15. Supplementary Tables Continued (For Description and Units, See the Caption of Table A-1; See Footnotes in Table A-12 for Coordinate Information.)

	<i>R</i>	4.25	4.50	4.50	4.50	4.50	4.50	4.50	4.50	4.50	4.75	4.75
β_1	180	135	90	45	0	45	90	135	180	135	90	45
γ_1	0.15	60.15	60.15	60.15	0.15	0.15	0.15	0.15	0.15	60.15	60.15	60.15
β_2	116.67	116.67	116.67	116.67	116.67	116.67	116.67	116.67	116.67	116.67	116.67	116.67
α_2	359.98	359.98	359.98	359.98	359.98	359.98	359.98	359.98	359.98	359.98	359.98	359.98
$E_{\text{int}}^{\text{HF}}$	3.64	-1.09	-0.79	3.46	3.58	1.69	-0.69	-1.07	1.11	-0.95	-0.69	1.34
$E_{\text{pol}}^{(1)}$	-4.22	-1.30	-0.89	-1.97	-1.19	-1.16	-0.70	-1.28	-2.11	-1.01	-0.70	-0.83
$E_{\text{exch}}^{(10)}$	8.72	0.34	0.20	6.18	5.28	3.16	0.08	0.35	3.71	0.15	0.08	2.54
$E_{\text{ind,resp}}^{(20)}$	-3.28	-0.22	-0.11	-2.00	-1.41	-0.81	-0.07	-0.21	-1.36	-0.12	-0.07	-0.77
$E_{\text{exch-ind,resp}}^{(20)}$	2.77	0.10	0.03	1.68	1.19	0.68	0.01	0.11	1.03	0.04	0.01	0.59
δ	-0.34	-0.02	-0.02	-0.43	-0.29	-0.18	-0.01	-0.02	-0.16	-0.01	-0.01	-0.19
$\varepsilon_{\text{pol,resp}}^{(1)}$	-0.26	0.20	0.17	-0.10	-0.27	-0.04	-0.15	0.20	-0.10	0.16	0.14	-0.04
$\varepsilon_{\text{exch}}^{(1)}(2)$	0.93	0.03	0.03	0.49	0.54	0.33	0.02	0.03	0.52	0.02	0.01	0.25
$tE_{\text{ind}}^{(22)}$	-0.58	0.01	0.00	-0.19	-0.17	-0.10	0.00	0.01	-0.25	0.01	0.00	-0.08
$tE_{\text{exch-ind}}^{(22)}$	0.48	-0.01	0.00	0.16	0.15	0.09	0.00	-0.01	0.19	0.00	0.00	0.06
$E_{\text{disp}}^{(20)}$	-3.36	-0.73	-0.60	-2.44	-2.76	-1.87	-0.50	-0.72	-2.06	-0.50	-0.41	-1.49
$E_{\text{disp}}^{(21)}$	0.84	0.18	0.13	0.31	0.37	0.26	0.12	0.18	0.51	0.13	0.09	0.18
$E_{\text{disp}}^{(22)}$	-0.96	-0.19	-0.16	-0.47	-0.54	-0.38	-0.14	-0.19	-0.60	-0.13	-0.11	-0.30

Table A-15. Supplementary Tables Continued (For Description and Units, See the Caption of Table A-1; See Footnotes in Table A-12 for Coordinate Information.) (continued)

$\varepsilon_{\text{disp}}^{(2)}$	-0.12	-0.01	-0.03	-0.16	-0.17	-0.12	-0.01	0.00	-0.10	0.00	-0.02	-0.12
$E_{\text{disp}}^{(2)}$	-3.48	-0.73	-0.63	-2.60	-2.93	-1.99	-0.52	-0.73	-2.16	-0.50	-0.43	-1.61
$E_{\text{exch-disp}}^{(20)}$	0.60	0.03	0.02	0.34	0.32	0.20	0.01	0.03	0.28	0.01	0.01	0.15
E_{int} ^{corr}	-2.30	-0.46	-0.41	-1.91	-2.36	-1.52	-0.34	-0.46	-1.52	-0.30	-0.27	-1.26
E_{int}	1.34	-1.55	-1.20	1.55	1.22	0.17	-1.03	-1.53	-0.41	-1.25	-0.96	0.07
$E_{\text{disp}}^{(20)(+\text{mb})}$	-4.02	-0.84	-0.66	-2.85	-3.39	-2.17	-0.55	-0.84	-2.43	-0.57	-0.45	-1.72
$E_{\text{int}}^{(+\text{mb})}$	0.68	-1.67	-1.26	1.14	0.59	-0.13	-1.07	-1.64	-0.78	-1.32	-0.99	-0.15

<u>NO. OF COPIES</u>	<u>ORGANIZATION</u>	<u>NO. OF COPIES</u>	<u>ORGANIZATION</u>
2	DEFENSE TECHNICAL INFORMATION CENTER DTIC DDA 8725 JOHN J KINGMAN RD STE 0944 FT BELVOIR VA 22060-6218	1	DIRECTOR US ARMY RESEARCH LAB AMSRL D D R SMITH 2800 POWDER MILL RD ADELPHI MD 20783-1197
1	HQDA DAMO FDT 400 ARMY PENTAGON WASHINGTON DC 20310-0460	1	DIRECTOR US ARMY RESEARCH LAB AMSRL DD 2800 POWDER MILL RD ADELPHI MD 20783-1197
1	OSD OUSD(A&T)/ODDDR&E(R) R J TREW THE PENTAGON WASHINGTON DC 20301-7100	1	DIRECTOR US ARMY RESEARCH LAB AMSRL CI AI R (RECORDS MGMT) 2800 POWDER MILL RD ADELPHI MD 20783-1145
1	DPTY CG FOR RDA US ARMY MATERIEL CMD AMCRDA 5001 EISENHOWER AVE ALEXANDRIA VA 22333-0001	3	DIRECTOR US ARMY RESEARCH LAB AMSRL CI LL 2800 POWDER MILL RD ADELPHI MD 20783-1145
1	INST FOR ADVNCED TCHNLGY THE UNIV OF TEXAS AT AUSTIN PO BOX 202797 AUSTIN TX 78720-2797	1	DIRECTOR US ARMY RESEARCH LAB AMSRL CI AP 2800 POWDER MILL RD ADELPHI MD 20783-1197
1	DARPA B KASPAR 3701 N FAIRFAX DR ARLINGTON VA 22203-1714		<u>ABERDEEN PROVING GROUND</u>
1	NAVAL SURFACE WARFARE CTR CODE B07 J PENNELL 17320 DAHLGREN RD BLDG 1470 RM 1101 DAHLGREN VA 22448-5100	4	DIR USARL AMSRL CI LP (BLDG 305)
1	US MILITARY ACADEMY MATH SCI CTR OF EXCELLENCE MADN MATH MAJ HUBER THAYER HALL WEST POINT NY 10996-1786		

NO. OF COPIES ORGANIZATION

ABERDEEN PROVING GROUND

20 DIR USARL
AMSRL WM BD
B E FORCH
W R ANDERSON
S W BUNTE
C F CHABALOWSKI
A COHEN
R DANIEL
D DEVYNCK
R A FIFER
B E HOMAN
A J KOTLAR
K L MCNESBY
M MCQUAID
M S MILLER
A W MIZOLEK
J B MORRIS
R A PESCE-RODRIGUEZ
B M RICE
R C SAUSA
M A SCHROEDER
J A VANDERHOFF

REPORT DOCUMENTATION PAGE			Form Approved OMB No. 0704-0188
<p>Public reporting burden for this collection of information is estimated to average 1 hour per response, including the time for reviewing instructions, searching existing data sources, gathering and maintaining the data needed, and completing and reviewing the collection of information. Send comments regarding this burden estimate or any other aspect of this collection of information, including suggestions for reducing this burden, to Washington Headquarters Services, Directorate for Information Operations and Reports, 1215 Jefferson Davis Highway, Suite 1204, Arlington, VA 22202-4302, and to the Office of Management and Budget, Paperwork Reduction Project(0704-0188), Washington, DC 20503.</p>			
1. AGENCY USE ONLY (Leave blank)	2. REPORT DATE	3. REPORT TYPE AND DATES COVERED	
	September 2000	Final, June 1996-May 1998	
4. TITLE AND SUBTITLE		5. FUNDING NUMBERS	
Investigation of the CH ₃ CN-CO ₂ Potential Energy Surface (PES) Using Symmetry-Adapted Perturbation Theory (SAPT)		622618.H80	
6. AUTHOR(S)			
Hayes L. Williams, Betsy M. Rice, and Cary F. Chabalowski			
7. PERFORMING ORGANIZATION NAME(S) AND ADDRESS(ES)		8. PERFORMING ORGANIZATION REPORT NUMBER	
U.S. Army Research Laboratory ATTN: AMSRL-WM-BD Aberdeen Proving Ground, MD 21005-5066		ARL-TR-2301	
9. SPONSORING/MONITORING AGENCY NAMES(S) AND ADDRESS(ES)		10. SPONSORING/MONITORING AGENCY REPORT NUMBER	
11. SUPPLEMENTARY NOTES			
12a. DISTRIBUTION/AVAILABILITY STATEMENT		12b. DISTRIBUTION CODE	
Approved for public release; distribution is unlimited.			
13. ABSTRACT (Maximum 200 words)			
<p>Symmetry-adapted perturbation theory (SAPT) has been used to investigate the intermolecular potential energy surface (PES) of CH₃CN-CO₂. A SAPT computation was performed for approximately 200 geometrical configurations using both a coarse grid in the five intermolecular coordinates as well as selected representative cuts. Four near-local minima are located on the PES. The deepest of these is -2.90 kcal/mol.</p>			
14. SUBJECT TERMS		15. NUMBER OF PAGES	
intermolecular interactions, symmetry adapted perturbation theory, quantum chemistry		86	
		16. PRICE CODE	
17. SECURITY CLASSIFICATION OF REPORT	18. SECURITY CLASSIFICATION OF THIS PAGE	19. SECURITY CLASSIFICATION OF ABSTRACT	20. LIMITATION OF ABSTRACT
UNCLASSIFIED	UNCLASSIFIED	UNCLASSIFIED	UL

INTENTIONALLY LEFT BLANK.

USER EVALUATION SHEET/CHANGE OF ADDRESS

This Laboratory undertakes a continuing effort to improve the quality of the reports it publishes. Your comments/answers to the items/questions below will aid us in our efforts.

1. ARL Report Number/Author ARL-TR-2301 (Williams) Date of Report September 2000

2. Date Report Received _____

3. Does this report satisfy a need? (Comment on purpose, related project, or other area of interest for which the report will be used.) _____

4. Specifically, how is the report being used? (Information source, design data, procedure, source of ideas, etc.) _____

5. Has the information in this report led to any quantitative savings as far as man-hours or dollars saved, operating costs avoided, or efficiencies achieved, etc? If so, please elaborate. _____

6. General Comments. What do you think should be changed to improve future reports? (Indicate changes to organization, technical content, format, etc.) _____

	Organization
CURRENT ADDRESS	Name
	E-mail Name
	Street or P.O. Box No.
City, State, Zip Code	

7. If indicating a Change of Address or Address Correction, please provide the Current or Correct address above and the Old or Incorrect address below.

	Organization
OLD ADDRESS	Name
	Street or P.O. Box No.
	City, State, Zip Code

(Remove this sheet, fold as indicated, tape closed, and mail.)
(DO NOT STAPLE)